






# IL-12 drives the expression of the inhibitory receptor NKG2A on human tumor-reactive CD8 T cells

Received: 27 February 2024

Accepted: 5 November 2024

Published online: 18 November 2024



Olivier Fesneau, Kimberly A. Samson , Wesley Rosales , Bretton Jones, Tarsem Moudgil, Bernard A. Fox , Venkatesh Rajamanickam  & Thomas Duhen  

Blockade of NKG2A/HLA-E interaction is a promising strategy to unleash the anti-tumor response. Yet the role of NKG2A<sup>+</sup> CD8 T cells in the anti-tumor response and the regulation of NKG2A expression on human tumor-infiltrating T cells are still poorly understood. Here, by performing CITE-seq on T cells derived from head and neck squamous cell carcinoma and colorectal cancer, we show that NKG2A expression is induced on CD8 T cells differentiating into cytotoxic, CD39<sup>+</sup>CD103<sup>+</sup> double positive (DP) cells, a phenotype associated with tumor-reactive T cells. This developmental trajectory leads to TCR repertoire overlap between the NKG2A<sup>−</sup> and NKG2A<sup>+</sup> DP CD8 T cells, suggesting shared antigen specificities. Mechanistically, IL-12 is essential for the expression of NKG2A on CD8 T cells in a CD40/CD40L- dependent manner, in conjunction with TCR stimulation. Our study thus reveals that NKG2A is induced by IL-12 on human tumor-reactive CD8 T cells exposed to a TGF- $\beta$ -rich environment, highlighting an underappreciated immuno-regulatory feedback loop dependent on IL-12 stimulation.

We and others have shown that the CD8<sup>+</sup> T cell infiltrate in human solid tumors is heterogenous, and consists of bystander T cells, tissue resident T cells and tumor-reactive T cells<sup>1–3</sup>. The latter, which are characterized by the co-expression of the cell surface markers CD39 and CD103 (DP CD8), are the main effectors of the anti-tumor response due to their capacity to recognize directly tumor antigens presented by MHC class I molecules at the surface of tumor cells<sup>4–6</sup>. However, their chronic stimulation in the tumor microenvironment (TME) can lead to the sustained expression of immune-regulatory molecules such as PD-1, CD39 and CTLA-4 (among others) that negatively impact their cytotoxic abilities, which can be further impaired by the presence of local soluble factors such as transforming growth factor beta (TGF- $\beta$ )<sup>7,8</sup>. Therefore, identifying strategies to unleash tumor-reactive T cells and thus restore and enhance the anti-tumor response has been a central goal to improve patient survival.

In that context, the targeting of the immune checkpoint molecules PD-1 / PD-L1 or CTLA-4 has led to dramatic responses in some

patients with metastatic cancers who had failed previous treatments<sup>9–11</sup>. However, responses have been observed primarily in cancers with high mutation load, such as melanoma, non-small cell lung cancer, and mismatch repair deficient (MMR-d) cancers, indicating a need for more effective therapies alongside clinically relevant biomarkers to stratify and improve treatment outcomes for patients. The absence of response to immunotherapy suggests that, for most cancers, multiple layers of inhibitory mechanisms exist and overcoming those hurdles will likely require targeting more than one pathway to restore a potent anti-tumor response.

Preclinical models have shown that blockade of the NKG2A/HLA-E pathway in combination with a cancer vaccine or an anti-PD-L1 blocking antibody might be a promising approach to improve patient's response to immunotherapy and this strategy is currently being evaluated in cancer patients<sup>6,12,13</sup>. NKG2A, a member of the killer immunoglobulin receptor (KIR) family, is an inhibitory receptor<sup>12,14,15</sup>. It forms a heterodimer with CD94, which is expressed at the surface of

Earle A. Chiles Research Institute, Providence Cancer Institute, Portland, OR, USA. ✉ e-mail: [thomas.duhen@providence.org](mailto:thomas.duhen@providence.org)

the cells. The ligand for NKG2A is the unconventional MHC-I molecule HLA-E<sup>16</sup> expressed at low levels in normal tissue, but that can be overexpressed in various cancers<sup>17</sup>. HLA-E expression is associated with worse prognosis in patients with breast cancer, colorectal cancer (CRC), non-small cell lung cancer, head and neck squamous cell carcinoma (HNSCC) and gynecological cancers<sup>18–20</sup>.

In contrast to other checkpoint molecules, NKG2A is expressed primarily by cytotoxic effectors of the anti-tumor response such as NK cells, CD8  $\alpha\beta$  T cells, and  $\gamma\delta$  T cells<sup>21–27</sup>, thus limiting the potential off-target effects when pursuing NKG2A blockade as treatment. To take full advantage of this pathway, key questions regarding the nature of the NKG2A-expressing CD8 T cells, their spatial distribution in the TME and the signals that drive NKG2A expression on CD8 T cells need to be clarified. Indeed, the absence of NKG2A upregulation on naïve CD8 T cells after TCR stimulation and exposure to TGF- $\beta$  (our preliminary data) implies that other requisite signals need to be identified. Our study reveals that NKG2A is expressed on tumor-infiltrating CD8 T cells (CD8 TILs) with a high cytotoxic potential and those cells recognize tumor antigens, highlighting the potential value of targeting them in patients. Furthermore, our results identify IL-12 as a key cytokine in the induction of NKG2A expression on CD8 T cells in the TME, demonstrating a previously underappreciated immuno-regulatory feedback loop dependent on IL-12 stimulation.

## Results

### Tumor-infiltrating NKG2A<sup>+</sup> CD8 T cells are prominent among cells with a tumor-reactive phenotype

We first analyzed the expression of NKG2A on CD8 T cells in the blood and tumor of patients with HNSCC and CRC by high dimensional flow cytometry (Suppl Fig. 1). We observed that, while NKG2A<sup>+</sup> CD8 T cells were present in the periphery, there was a higher frequency of those cells in the tumor for both cancers (Fig. 1a and b and Suppl Fig. 2a and b). To explore the nature of NKG2A<sup>+</sup> CD8 T cells further, we examined the expression of CD39, CD103 and other cell surface markers associated with costimulation, memory, tissue residency and activation/exhaustion. This approach led to the manual identification of five subsets of NKG2A<sup>+</sup> CD8 T cells, two in the blood (B1 and B2) and three in the tumor (T1, T2, and T3) in patients with HNSCC and CRC (Fig. 1c, d and e and Suppl Fig. 2c, d and e). An additional subset that co-expressed CD103 was detected in the blood but was not further analyzed due to its very limited presence. The two subsets in the blood lacked CD39, CD103, PD-1 and CD69 and differed based on the expression of CD28, CD127 and CD45RA (Fig. 1f and Suppl Fig. 2f). Cells in the B1 subset displayed a phenotype reminiscent of terminally differentiated effector memory T cells (or TEMRA). In contrast, cells in the B2 subset resembled memory CD8 T cells. The composition of NKG2A<sup>+</sup> CD8 T cells in tumor was more heterogeneous. The subsets T1 and T2 expressed CD103 and CD69, markers of tissue resident cells, but differed for most of the remaining markers. Cells in the T1 subset showed high levels of CD39 and PD-1, a phenotype of tumor-reactive CD8 T cells, also associated with T-cell exhaustion<sup>1,4,5</sup>. Cells in the T2 subset displayed intermediate levels of PD-1 and expressed heterogeneous levels of CD39, CD28, and CD127, a phenotype consistent with tissue resident memory T cells<sup>28–30</sup>. Cells in the T3 subset lacked both CD39 and CD103 and more closely resembled cells from the B2 subset in the blood. Based on our results, T1 cells had a phenotype consistent with DP CD8 (CD39<sup>+</sup>CD103<sup>+</sup>), while T2 cells and T3 cells shared phenotypic characteristics with SP CD8 (CD39<sup>+</sup>CD103<sup>+</sup>) and DN CD8 (CD39<sup>+</sup>CD103<sup>+</sup>) TILs, respectively. Next, we analyzed the proportion of DN, SP and DP CD8 in NKG2A<sup>+</sup> and NKG2A<sup>+</sup> CD8 TILs in HNSCC and CRC tumors (Fig. 1g and Suppl Fig. 2g). This analysis revealed statistically significant differences between NKG2A<sup>+</sup> and NKG2A<sup>+</sup> CD8 TILs, with NKG2A<sup>+</sup> cells containing primarily DN CD8 T cells while NKG2A<sup>+</sup> cells were enriched in DP CD8 T cells. Interestingly, tumors from patients with human papilloma virus (HPV)-driven HNSCC

demonstrated a significantly lower frequency of NKG2A<sup>+</sup> cells in DP CD8 TILs as compared to HPV-negative HNSCC tumors (Fig. 1h). Altogether, our results indicate that in HNSCC and CRC tumors NKG2A is mainly expressed by DP CD8 TILs.

### NKG2A<sup>+</sup> DP CD8 TILs are terminally differentiated and transcriptionally distinct from NKG2A<sup>+</sup> DP CD8 TILs

To further understand the biology of NKG2A<sup>+</sup> CD8 T cells in tumors, we sorted the CD3<sup>+</sup> T cells from 6 patients with HNSCC and 5 patients with MMR-p CRC and analyzed their transcriptomes at the single cell level by performing cellular indexing of transcriptomes and epitopes (CITE-seq). Using barcoded antibodies specific for CD8, CD39 and CD103, we identified the three main CD8 TIL subsets, namely CD39<sup>+</sup>CD103<sup>+</sup> (DN CD8), CD39<sup>+</sup>CD103<sup>+</sup> (SP CD8) and CD39<sup>+</sup>CD103<sup>+</sup> (DP CD8) recapitulating our previous observations by flow cytometry<sup>1</sup> (Fig. 2a and Suppl Fig. 3a). This approach, combined with the unsupervised clustering of the cells (RNA + ADT), identified a degree of heterogeneity among the three CD8 T cell subsets (Fig. 2b and c and Suppl Fig. 3b and c). In the HNSCC dataset, each CD8 subset comprised multiple subclusters; DN CD8 were enriched in clusters 0, 3 and 5, SP CD8 enriched in clusters 1, 4 and 6 and DP CD8 enriched in clusters 2 and 7. This was corroborated by gene expression signatures associated with each cluster. Within the DN CD8, cluster 3 exhibited a gene signature associated with naïve/central memory CD8 T cells (*LEF1*, *KLF2*, *TCF7*), and clusters 0 and 5 expressed genes characteristic of CD8 T effector memory (TEM)/terminally differentiated effector memory (TEMRA) cells such as *KLRG1*, *EOMES* and *GZMK*. SP CD8 clusters displayed high expression of *ITGAE* (CD103), *ZNF683* (encoding Hobit), and *IL7R* and low expression of *KLF2*, a gene expression pattern consistent with tissue resident memory T cells. In contrast, DP CD8 TIL clusters (2 and 7) demonstrated high expression of genes expressed by activated/exhausted T cells (such as *ENTPD1* and *PDCD1*), indicative of chronic TCR stimulation in the tumor, but also high expression of *KLRC1* (NKG2A). The analysis of our CRC dataset also demonstrated a degree of heterogeneity among the CD8 T cell subsets, with SP CD8 composed of clusters 2 and 4, and DP CD8 enriched in clusters 1, 3, 5 and 6. DN CD8 T cells were the only subset represented by a unique cluster, namely cluster 0 (Suppl Fig. 3b and c).

To understand the differentiation trajectories of CD8 T cells in the TME, we first assessed the expression signatures of naïve/TCM and activated/exhausted T cells for each cluster. For the HNSCC dataset, this analysis identified cluster 3 as the least differentiated cells (highest naïve/TCM score) while clusters 2 and 7 contained highly differentiated cells (highest activation/exhaustion score) (Fig. 2d). RNA velocity, which predicts the progression of a current cellular state toward a future state based on RNA splicing, further supported cluster 3 as an initial state and revealed two main terminal states, one in cluster 6 (SP CD8) and one in cluster 7 (DP CD8) (Fig. 2e, f and g). Of note, cluster 4 might represent a transitional state from which cells can differentiate into SP CD8 or DP CD8. The gene expression analysis over latent time for the lineage 7 trajectory revealed a rapid downregulation of “naïve/memory” genes such as *SELL*, *LEF1*, *TCF7* and an increase in genes associated with tissue residency (*ITGAE*) and activation/exhaustion (*PDCD1*, *CTLA4*, *HAVCR2*, *ENTPD1*, *TOX*) (Fig. 2h and i). Interestingly, we observed an increase in effector genes such as *GZMK* and *EOMES* which were downregulated as cells further differentiated. Most importantly, progression over latent time correlated with increase in *KLRC1* (NKG2A) expression, together with effector genes (*IFNG*, *GZMB*, *GNLY*). Using a similar approach for the CRC dataset, we identified cluster 0 as the initial state and two main terminal states, one in cluster 2 (SP CD8) and one in cluster 3 (DP CD8) (Suppl Fig. 3d, e, f and g). The gene expression analysis over latent time for the lineage 3 trajectory also revealed a rapid downregulation of naïve/memory

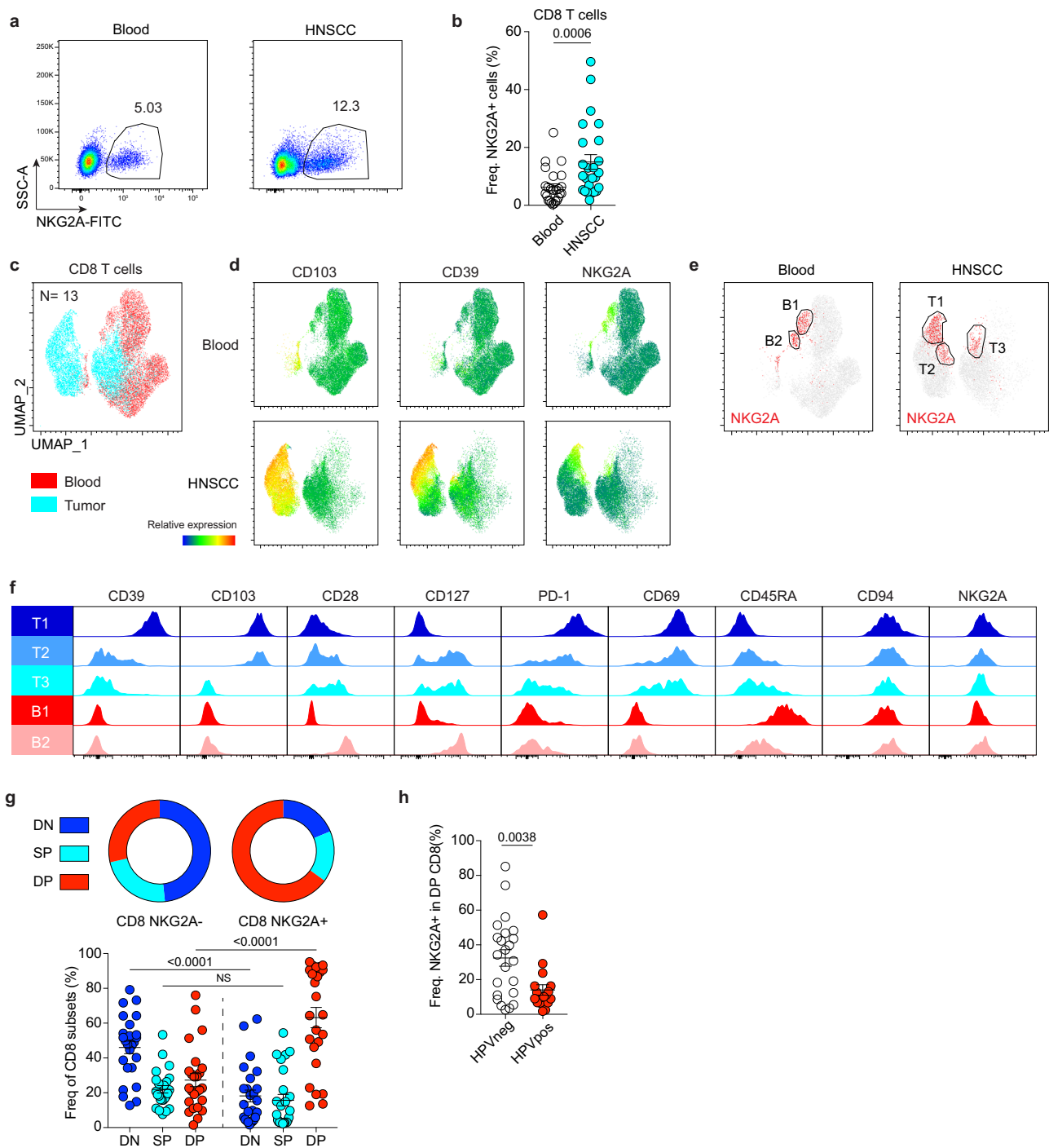


**Fig. 1 | NKG2A<sup>+</sup> cells are enriched in CD103<sup>+</sup> CD39<sup>+</sup> (DP) CD8 T cells in HNSCC tumors.** **a** Flow cytometry analysis and **(b)** summary of NKG2A expression by CD8 T cells from the blood and the tumor of HNSCC patients (n=25). **c** Unsupervised clustering of blood (red) and tumor-infiltrating (cyan) CD3<sup>+</sup> CD8<sup>+</sup> T cells isolated from 13 HNSCC patients. **d** Normalized expression of CD103, CD39 and NKG2A on CD8 T cells from blood and tumor. **e** NKG2A expression on blood and tumor CD8 T cells (positive cells are shown as red dots), with B1 and B2 representing subsets of NKG2A<sup>+</sup> cells in the blood, and T1, T2 and T3 representing subsets of NKG2A<sup>+</sup> cells in

the tumor. **f** Phenotype of the different subsets of NKG2A<sup>+</sup> CD8 T cells (n=13). **g** Frequency of DN (CD39<sup>+</sup> CD103<sup>-</sup>), SP (CD39<sup>-</sup> CD103<sup>+</sup>) and DP (CD39<sup>+</sup> CD103<sup>+</sup>) cells among NKG2A<sup>-</sup> (left) and NKG2A<sup>+</sup> (right) CD8 TILs in HNSCC patients (n=25). **h** Summary of the expression of NKG2A by DP CD8 TILs in HPV<sup>-</sup> (n=23) and HPV<sup>+</sup> (n=18) HNSCC patients. Horizontal lines indicate the mean ± SEM. NS= not significant; p-values were determined by paired 2-tailed t test (**b**), by one-way analysis of variance with Tukey's post hoc testing (**g**), or unpaired 2-tailed t test (**h**).

genes and the increase in genes associated with tissue residency and activation/exhaustion. Importantly, the increase in *KLRC1* (NKG2A) expression also correlated with an increase in effector genes in that dataset (Suppl Fig. 3h and i). Overall, our analysis revealed that in the tumor, the NKG2A<sup>+</sup> DP CD8 are terminally differentiated and exhibit a high cytotoxic potential.

### NKG2A<sup>+</sup> DP CD8 TILs are enriched in the tumor intraepithelial compartment

We and others have previously shown that CD103<sup>+</sup> CD8 TILs are enriched in the tumor intraepithelial compartment (TIC) where they can directly recognize and kill tumor cells<sup>1,4,5,31–35</sup>. Because NKG2A expression on DP CD8 TILs correlates with late-stage differentiation

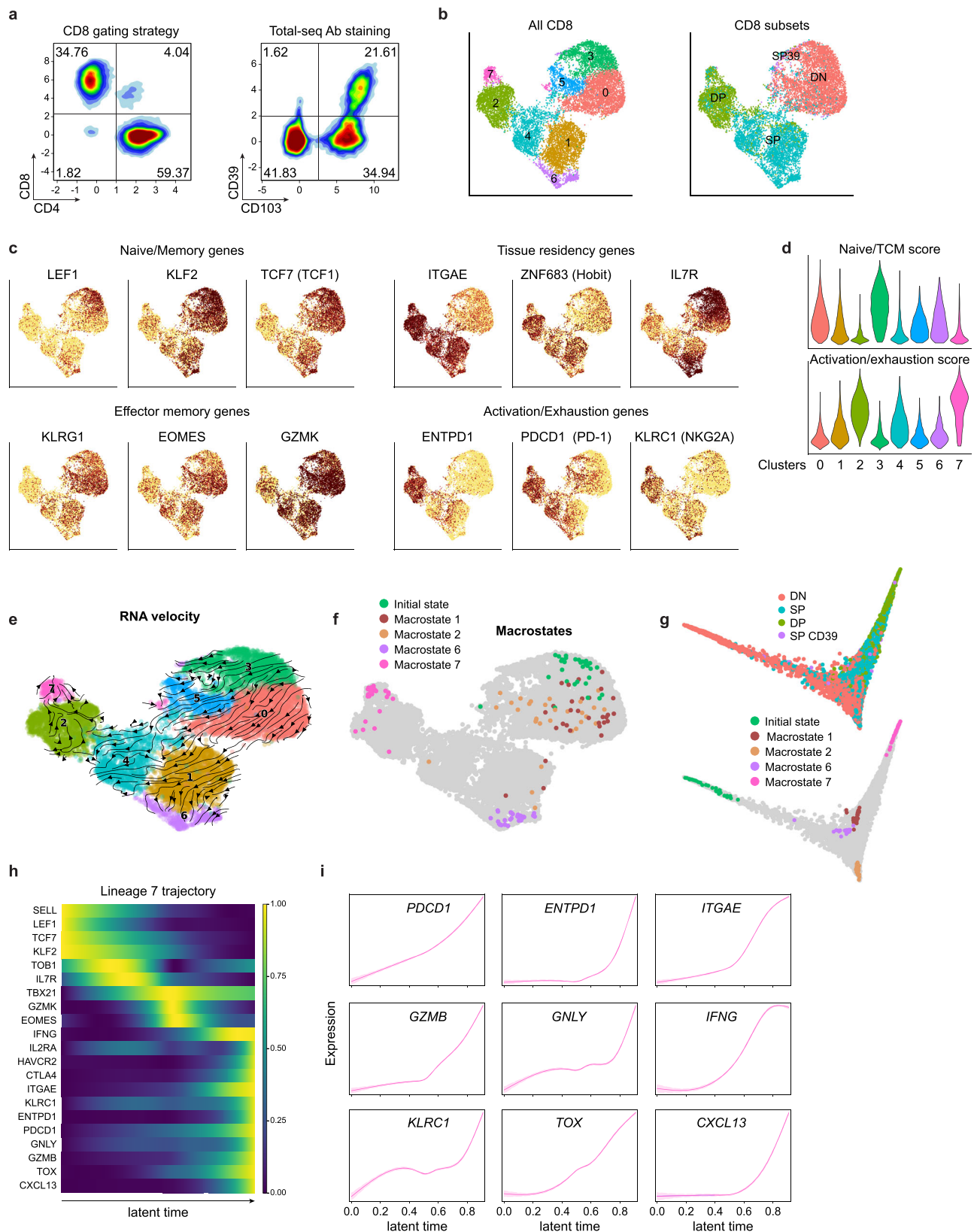


**Fig. 2 | CD8 TILs are heterogeneous and contain a subset of cytotoxic cells expressing NKG2A.** **a** Gating strategy of CD8 T cells (left) and CD8 T cell subsets (right) using CITE-seq antibodies. **b** Unsupervised clustering of CD8 T cells from TILs (left) and projection of the 3 CD8 subsets identified in (b) onto the UMAP plot (right) ( $n = 6$  HNSCC patients). **c** Normalized expression of selected markers defining tumor CD8 T cell clusters. **d** Naive/TCM and Activation/exhaustion scores for each cell cluster. **e** RNA velocity of CD8 T cells projected on the UMAP plot.

Arrows indicate the putative differentiation direction. Arrow sizes indicate the magnitude of predicted directionality. **f** Highlight of the cells most confidently assigned to each initial and terminal state on the UMAP. **g** Diffusion map of cells colored by CD8 subsets and microstates. **h** Gene expression dynamics of differentially expressed genes ordered along the latent time inferred by RNA velocity for the lineage 7. **i** Smoothed gene expression trends in pseudotime for the lineage 7.



and a high cytotoxic potential, we hypothesized that NKG2A<sup>+</sup> DP CD8 T cells might be enriched in the TIC where they could directly interact with tumor cells. To address that, tissue sections from patients with HNSCC and CRC were stained for CD39 and NKG2A (RNA) and CD8 (protein). While most CD8 T cells were detected in the tumor stroma, some CD8 T cells were also present in the TIC (Fig. 3a, b and c). CD8 T cells present in the TIC were more prone to express CD39 (Fig. 3d), and we observed an enrichment of NKG2A<sup>+</sup> cells among CD8<sup>+</sup>CD39<sup>+</sup> T cells in the TIC as compared to CD8<sup>+</sup>CD39<sup>+</sup> T cells in the stroma (Fig. 3e).

### TCR repertoire overlap between NKG2A<sup>−</sup> and NKG2A<sup>+</sup> DP CD8 TILs suggests a shared origin

Thus far, our results suggest that NKG2A is induced on CD8 TILs as they differentiate along the DP CD8 pathway. If that assumption is correct, the TCR repertoire of NKG2A<sup>−</sup> and NKG2A<sup>+</sup> DP CD8 should display some similarity. To address this, we performed a quantitative assessment of TCRβ clonotypes by deep sequencing of blood memory CD8 T cells, DN CD8, SP CD8, NKG2A<sup>−</sup> DP CD8 and NKG2A<sup>+</sup> DP CD8 TILs directly ex vivo. Our results revealed that, while the TCR repertoire of NKG2A<sup>+</sup> DP CD8 TILs showed little overlap with the TCR repertoire of blood memory CD8 T cells, DN CD8 and SP CD8 TILs, approximately half of its TCRβ clonotypes were shared with NKG2A<sup>−</sup> DP CD8 TILs (Fig. 4a). Calculation of the Morisita index, an abundance-based similarity index that determines the overlap between 2 cell populations, confirmed the high degree of overlap among TCRβ clonotypes in NKG2A<sup>−</sup> and NKG2A<sup>+</sup> DP CD8 TILs but not with the other CD8 TILs (Fig. 4b). Of note, most shared TCRβ clonotypes were present at comparable frequencies between NKG2A<sup>−</sup> and NKG2A<sup>+</sup> DP CD8, only a minority of shared TCRβ clonotypes expanded in one subset and not the other (Fig. 4c). Hence, our results support a common origin for both NKG2A<sup>−</sup> and NKG2A<sup>+</sup> DP CD8 TILs.

### NKG2A<sup>−</sup> and NKG2A<sup>+</sup> DP CD8 TILs recognize the same tumor antigens

Given the overlap in their TCR repertoire, we investigated whether NKG2A<sup>−</sup> and NKG2A<sup>+</sup> DP CD8 TILs recognized the same or distinct tumor antigens. First, we determined their capacity to recognize the E proteins of HPV16 in HPV<sup>+</sup> HNSCC patients. NKG2A<sup>−</sup> and NKG2A<sup>+</sup> DP CD8 TILs were sorted and expanded in vitro, and antigen reactivity was measured by 4-1BB up-regulation<sup>1,36–38</sup> after coculture with APCs electroporated with RNA encoding for E2, E5, E6 and E7 from HPV16 (Suppl Fig. 4a). Of note, phenotypic analysis of the expanded cells revealed that NKG2A expression was stable and was not induced by in vitro expansion (Suppl Fig. 5a and b). Using this approach, we found that reactivity to E6 was dominant and detected in 5/6 patients whereas reactivity to E2 and E7 was present in 3/6 and 1/6 patients, respectively (Fig. 5a and b and Suppl Fig. 6a). We did not detect any reactivity to E5 in our patient cohort. In accordance with the TCR repertoire analysis, HPV-reactive T cells were observed in both subsets although at varying frequencies. Furthermore, using overlapping single peptides for HPV16 E6, we showed for one patient that NKG2A<sup>−</sup> and NKG2A<sup>+</sup> DP CD8 TILs recognized the same E6 peptide (Fig. 5c and Suppl Fig. 6b). We also compared NKG2A<sup>−</sup> and NKG2A<sup>+</sup> DP CD8 TILs for their capacity to recognize tumor-specific somatic mutations for one HNSCC and one CRC patient. After whole exome sequencing and RNA sequencing of the patient's tumor, we assessed the reactivity of DP CD8 TILs against the identified mutations. Following this approach, we identified T-cell reactivity against two somatic mutations. For the HNSCC patient, DP CD8 TILs recognized a mutation in NOTCH1 while in the CRC patient a mutation in HEATR5A was recognized (Fig. 5d and Suppl Fig. 6b). Importantly, those two neoantigens were recognized by NKG2A<sup>−</sup> and NKG2A<sup>+</sup> DP CD8 TILs. Altogether,

our results indicate that both populations contain cells that can recognize the same antigens.

### NKG2A upregulation by CD8 T cells requires signals from CD4 T cells and MHC class II<sup>+</sup> cells

Both trajectory and TCR repertoire analyses suggest that tumor-reactive CD8 T cells acquire NKG2A while in the tumor. Thus, we sought to identify the factors driving its expression on CD8 T cells. Previous work had shown that NKG2A expression on CD8 T cells required TCR stimulation in the presence of TGF-β<sup>39,40</sup>. Those results were obtained by stimulating PBMC with staphylococcal enterotoxin B (SEB) and exogenous TGF-β as shown in Fig. 6a, and the level of NKG2A expression correlated with the SEB concentration (Suppl Fig. 7a). We obtained similar results with CytoStim but not with the mitogen phytohemagglutinin (PHA) reflecting the fact that different T cell activators trigger distinct signaling pathways (Fig. 6a and b and Suppl. Figure 4b). Stimulation of PBMCs with SEB and TGF-β also led to strong up-regulation of CD39 (Suppl Fig. 7b) and PD-1 (Suppl Fig. 7c). To refine this analysis, we stimulated sorted naïve CD8 T cells (NKG2A<sup>−</sup>) (Suppl Fig. 4c) with CD3/CD28 beads with or without TGF-β and analyzed NKG2A expression after 8 days of culture. Surprisingly these conditions did not lead to NKG2A induction on CD8 T cells, despite the cells being activated (Fig. 6c and d) and responsive to TGF-β as illustrated by CD103 up-regulation (Suppl Fig. 7d). Mechanistically, SEB triggers polyclonal stimulation by binding both the TCR and CD28 on T cells and MHC class II and B7 molecules on APCs<sup>41</sup>. Thus, additional factor(s) produced by myeloid cells and CD4 T cells might be responsible for the induction of NKG2A on CD8 T cells. To address that, we evaluated the role of these two cell types on NKG2A expression. First, we showed that depletion of CD4 T cells prior to SEB stimulation led to reduced expression of NKG2A on CD8 T cells but had no impact on their activation as demonstrated by CD25 expression (Fig. 6e and f). We also assessed the contribution of each cell type on NKG2A expression by incubating sorted naïve CD8 T cells together with autologous CD4 T cells, monocytes, or both in the presence of SEB with or without TGF-β (Suppl. Figure 4c and d). While the addition of monocytes and TGF-β led to some upregulation of NKG2A on CD8 T cells, the highest levels of NKG2A expression were observed when both CD4 T cells and monocytes were present in the culture (Fig. 6g). Of note, the limited effect of TGF-β observed here might be due to endogenous TGF-β secretion by monocytes as demonstrated by CD103 up-regulation on CD8 T cells (Suppl Fig. 7e). Overall, our results showed that TCR stimulation and TGF-β are not sufficient to induce de novo expression of NKG2A on CD8 T cells; monocytes and CD4 T cells provide required signals for its expression.

### IL-12 is essential to induce NKG2A expression on CD8 T cells

To identify the factor(s) that induce NKG2A expression on CD8 T cells, we developed a two-step in vitro assay to mimic the priming of CD8 T cells in the tumor-draining lymph node followed by their restimulation in the TME after migration via the blood. CD8 T cells were stimulated for 24 h with CD3/CD28 beads, at which point the beads were removed and the cells were kept in culture for 2 more days before restimulation with CD3/CD28 beads in the presence of various cytokines known to be secreted by activated monocytes. This approach identified IL-12 as the only cytokine that induced NKG2A expression on CD8 T cells, which was further increased by TGF-β (Fig. 7a and b and Suppl Fig. 4e). IL-12 also promoted CD8 T cell activation as illustrated by higher expression of CD39 on the cell surface (Suppl Fig. 8a, b) as shown recently<sup>42</sup>. To determine if IL-12 was involved in SEB-induced NKG2A up-regulation, we cultured PBMC with SEB in the presence or absence of an anti-IL-12p70 neutralizing antibody (Ab). Addition of the anti-IL-12p70 Ab significantly reduced NKG2A expression by CD8 T cells, supporting a role for IL-12 in SEB-mediated NKG2A expression on CD8 T cells (Fig. 7c and d). Because optimal secretion of IL-12 is

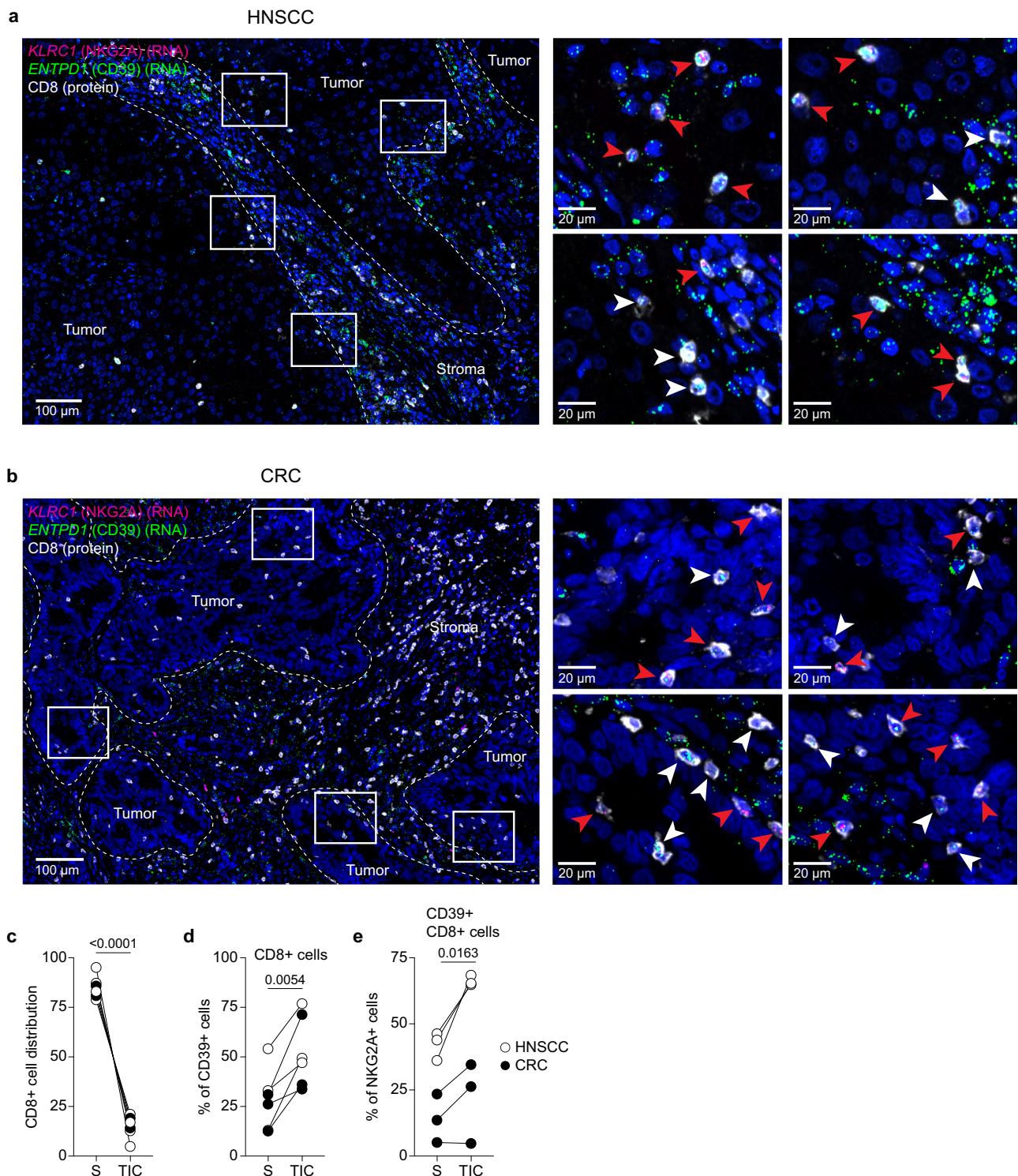


**Fig. 3 | NKG2A<sup>+</sup> CD39<sup>+</sup> CD8 are enriched in the tumor intraepithelial compartment.** ISH/IF for NKG2A (RNA, magenta), CD39 (RNA, green) and CD8 (protein, white) on an HNSCC tumor (a) and a CRC tumor (b). Representative low-power image together with high-power views of four selected areas are shown. CD8<sup>+</sup> CD39<sup>+</sup> NKG2A<sup>+</sup> cells are highlighted with red arrows, and CD8<sup>+</sup> CD39<sup>+</sup> NKG2A<sup>+</sup> cells are highlighted with white arrows. **c** Summary of the distribution of CD8<sup>+</sup> cells in the stroma (S) and tumor intraepithelial compartment

(TIC). **d** Percentages of CD39<sup>+</sup> cells among CD8<sup>+</sup> cells in the stroma (S) and tumor intraepithelial compartment (TIC). **e** Percentages of NKG2A<sup>+</sup> cells among CD39<sup>+</sup> CD8<sup>+</sup> cells in the stroma (S) and tumor intraepithelial compartment (TIC). The analysis was performed on 3 HNSCC tumors and 3 CRC tumors. Scale bar = 100  $\mu$ m for low-power images and 20  $\mu$ m for high-power views. *p*-values were determined by paired 2-tailed *t* test (**c**, **d** and **e**).

dependent on the CD40/CD40L pathway during CD4 T cell/APC interaction<sup>43,44</sup>, we repeated the experiment in the presence or absence of an anti-CD40 Ab. Our results showed that CD40 blockade also impaired NKG2A expression in response to SEB (Fig. 7c and d) and this

correlated with reduced secretion of IL-12 in the culture supernatant (Fig. 7e). We also evaluated the ability of IL-12 to up-regulate NKG2A on “terminally differentiated” tumor-reactive NKG2A<sup>+</sup> DP CD8 TILs after peptide-mediated TCR stimulation. First, NKG2A<sup>+</sup> DP CD8 T cells



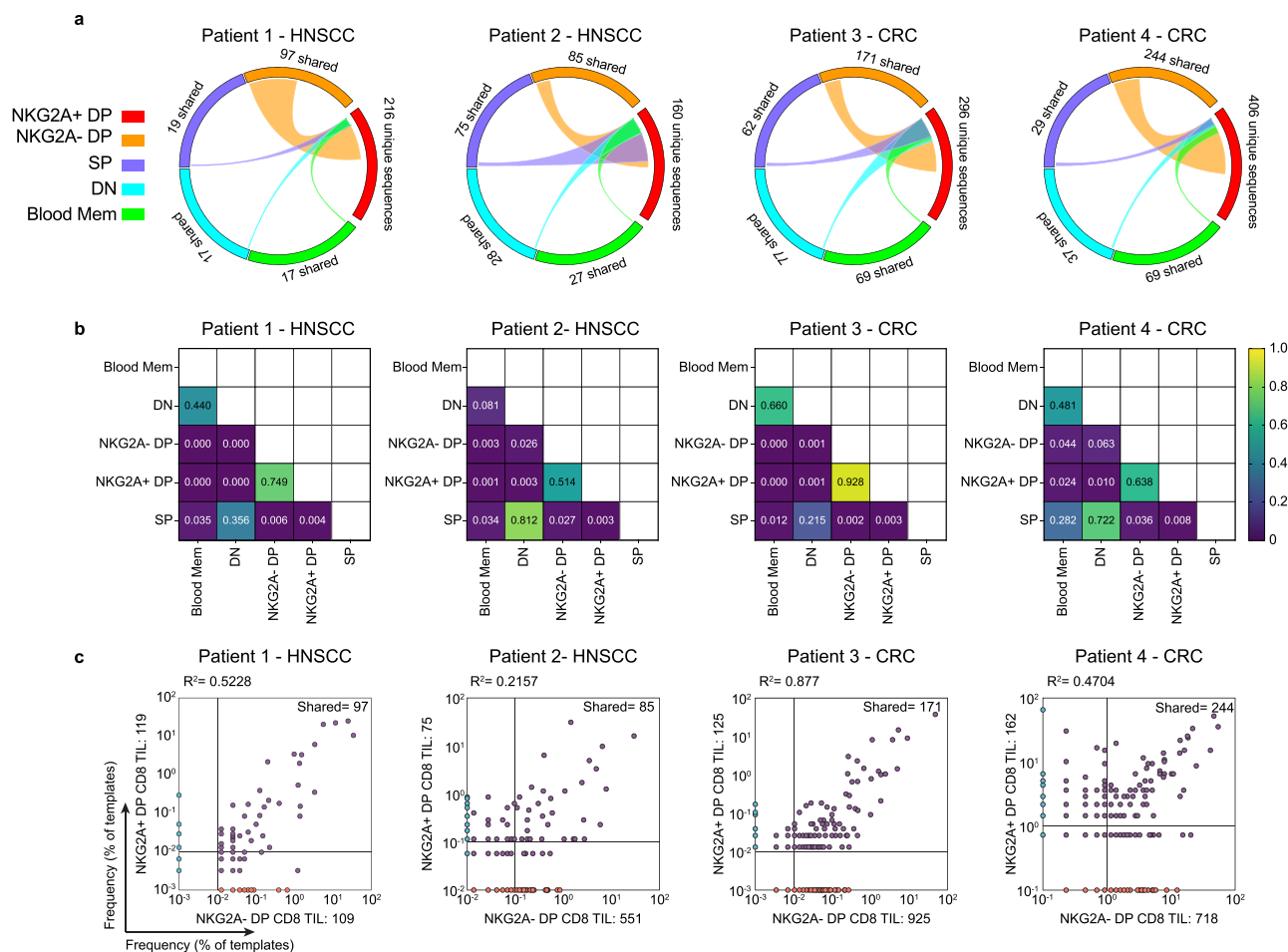


**Fig. 4 | The TCR repertoire of NKG2A<sup>+</sup> DP CD8 overlaps with NKG2A<sup>-</sup> DP CD8 T cells. **a**** Circos plot of unique productive TCR $\beta$  nucleotide sequence for each of the indicated cell populations. Connections highlight sequences from NKG2A<sup>+</sup> DP CD8 found in the other CD8 T cell populations. The number of shared sequences is indicated. **b** Similarities between the TCR repertoires of the different CD8 T cell subsets were measured using the Morisita-Horn index. **c** Scatter plot comparing the

TCR repertoire of NKG2A<sup>-</sup> and NKG2A<sup>+</sup> DP CD8 TILs. Each dot represents a unique TCR clonotype. Dots on either axis indicate clonotypes detected within a single repertoire; purple dots indicate clonotypes shared between the two CD8 T cell populations. This analysis was performed for 2 patients with HNSCC and 2 patients with CRC.

isolated from a patient's tumor were cultured with their cognate tumor peptide and the reactive T cells (identified by 4-1BB up-regulation) were sorted and expanded in vitro. The resulting peptide-specific NKG2A<sup>-</sup> DP CD8 T cells were then cultured with an HLA-matched tumor cell line pulsed with the cognate peptide in the presence or absence of exogenous IL-12. Under those culture conditions, the expression of NKG2A on CD8 T cells was induced only when exogenous IL-12 was present (Fig. 8a and b).

Finally, we inquired whether IL-12-expressing cells could be detected in the TME and determined their location in relation to CD8 T cells. To do so, we stained tumor tissue sections with *IL12B* and *TGFB1* RNAscope probes and a CD8 antibody. *IL12B* mRNA was detected in the TME, although in a small number of cells, and those cells were localized in the tumor stroma near the invasive margin (Fig. 8c). Interestingly, our results indicate that CD8 T cells can be found close to IL-12<sup>+</sup> cells in a TGF- $\beta$ -rich environment, consistent with the NKG2A-promoting culture conditions we identified (Fig. 8d). Altogether, our results suggest that IL-12 plays a central role in the induction of NKG2A on CD8 T cells following TCR stimulation.

## Discussion

In this study, we showed that NKG2A is expressed by some tumor-reactive CD8 T cells and identified IL-12 as a key cytokine required for its induction. NKG2A expression was not restricted to a specific CD8 T

cell subset in tumors. However, the dominant population of NKG2A<sup>+</sup> cells resembled the previously identified CD39<sup>+</sup> CD103<sup>+</sup> DP CD8 TILs<sup>1</sup>. Our analysis revealed that NKG2A expression by CD8 T cells increased as the cells differentiated into DP CD8 and acquired a cytotoxic potential. As a result, there was a high degree of shared TCR clonotypes among NKG2A<sup>-</sup> and NKG2A<sup>+</sup> DP CD8 TILs which correlated with recognition of some of the same tumor antigens. Interestingly, we found that TCR stimulation in the presence of TGF- $\beta$ , two signals known to drive NKG2A expression, were not sufficient to induce NKG2A expression on naïve CD8 T cells. Instead, we demonstrated that NKG2A expression required additional signals provided by APCs and CD4 T cells. We identified IL-12 secreted by APCs as a key cytokine in this process.

The rationale for NKG2A blockade in cancer patients rests on inhibition of the negative effects of HLA-E/NKG2A interactions. However, NKG2A expression by tumor-reactive CD8 T cells has been presumed but not yet demonstrated. Here, we report that NKG2A is expressed predominantly by cells of the DP CD8 phenotype, known to be enriched in cells that recognize tumor-associated and tumor-specific neoantigens<sup>1</sup>. Furthermore, these NKG2A<sup>+</sup> DP CD8 T cells had a high cytotoxic potential and were enriched in the tumor intraepithelial compartment in contact with tumor cells. Thus, anti-NKG2A blocking antibodies could reduce this inhibitory signal on tumor-reactive T cells under conditions in which the tumor cells or APCs express HLA-E and

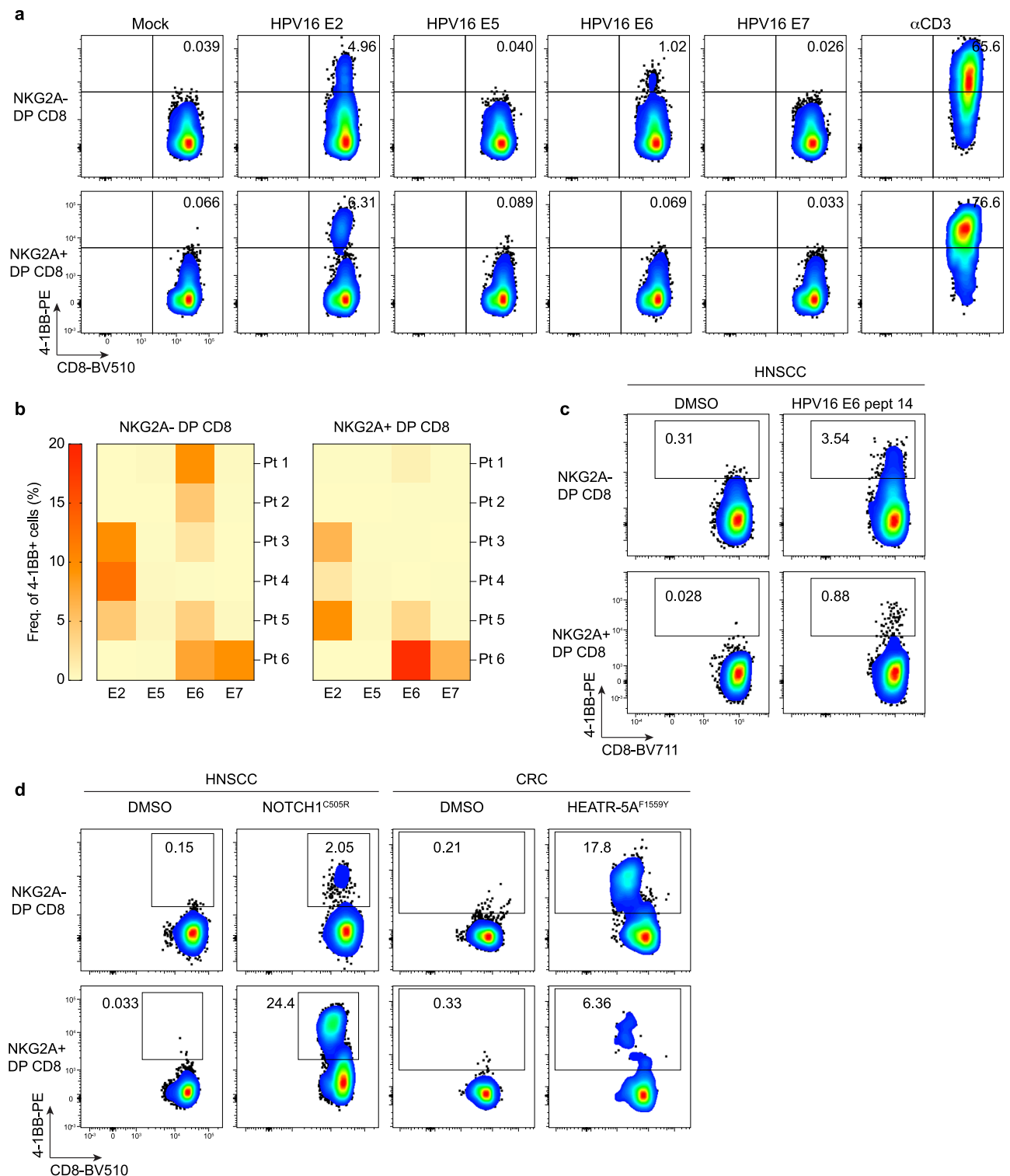


**Fig. 5 | Tumor antigen-reactive T cells are present in both NKG2A<sup>-</sup> and NKG2A<sup>+</sup> DP CD8 TILs. a** In vitro expanded CD8 TILs were cocultured with autologous APCs electroporated with the indicated HPV16 E constructs. T cell reactivity was assessed by 4-1BB upregulation after 20 hours of culture. Data for one representative patient with HPV<sup>+</sup> HNSCC are shown. **b** Summary of the reactivity of NKG2A<sup>-</sup> and NKG2A<sup>+</sup> DP CD8 TILs to HPV16 E proteins for 6 patients with HPV<sup>+</sup> HNSCC, as measured by 4-1BB upregulation. The colors in the heatmap legend

represent the frequency of 4-1BB<sup>+</sup> cells. **c** NKG2A<sup>-</sup> and NKG2A<sup>+</sup> DP CD8 TILs isolated from one HPV<sup>+</sup> HNSCC patient were cultured with autologous APCs pulsed with DMSO or the peptide 14 of the HPV16 E6 peptide pool and reactivity was measured by 4-1BB upregulation. **d** NKG2A<sup>-</sup> and NKG2A<sup>+</sup> DP CD8 TILs isolated from one HNSCC patient (left) and one CRC patient (right) were cultured with autologous APCs pulsed with DMSO or the indicated mutated peptide and reactivity was measured by 4-1BB upregulation.



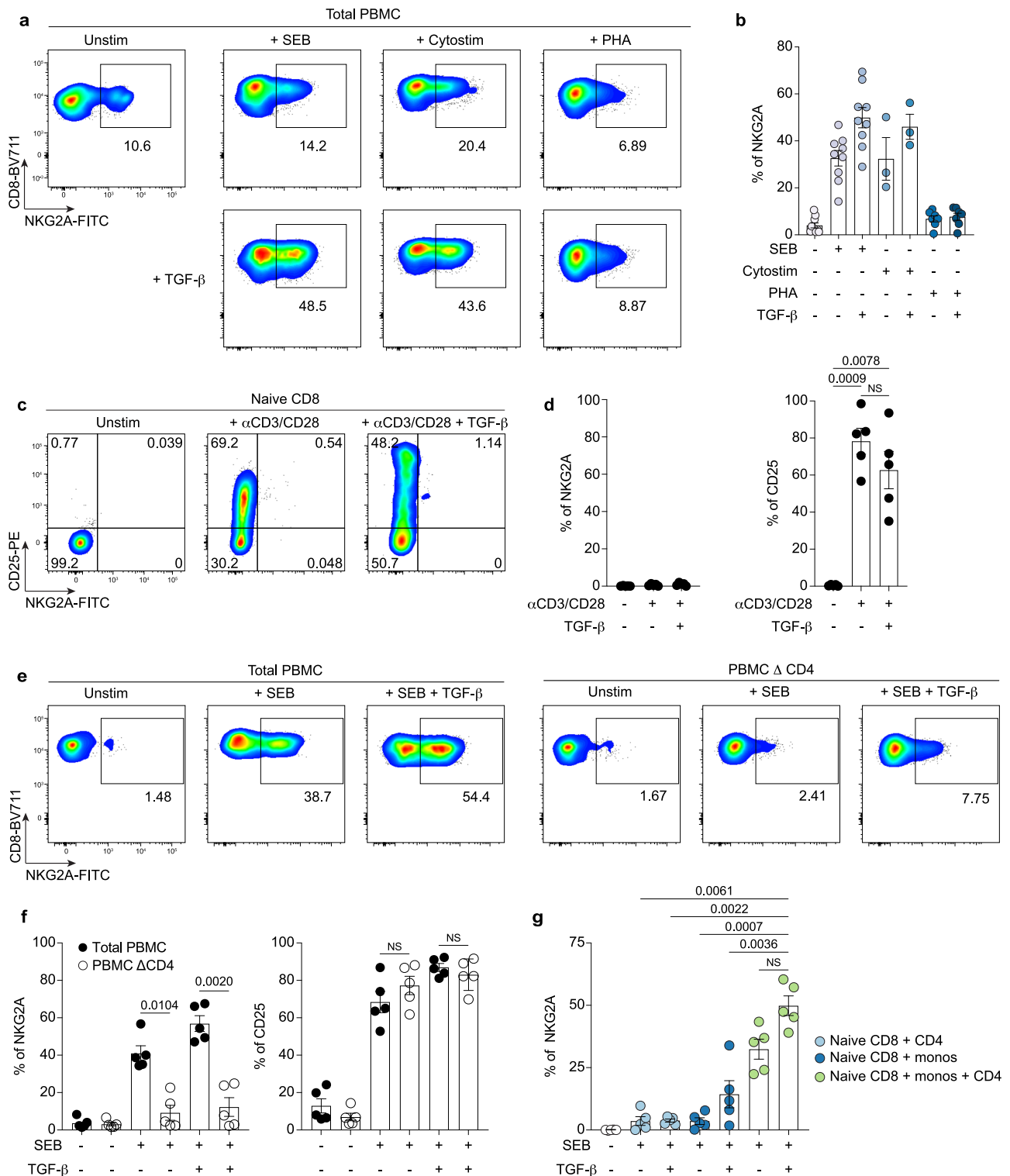


**Fig. 6 | Induction of NKG2A by CD8 T cells requires additional signals besides TCR stimulation and TGF-β.** **a** Flow cytometry analysis of one representative donor and **(b)** summary of NKG2A expression by CD8 T cells following PBMC stimulation with SEB ( $n=9$ ), Cytostim ( $n=3$ ) or PHA ( $n=7$ ) in the presence or absence of TGF-β. **c** Flow cytometry analysis and **(d)** summary of NKG2A and CD25 expression on sorted naive CD8 T cells stimulated with CD3/CD28 beads in the presence or absence of TGF-β ( $n=5$ ). **e** Flow cytometry analysis and **(f)** summary of NKG2A expression by CD8 T cells after stimulation of PBMCs or CD4-depleted

PBMCs with SEB in the presence or absence of TGF-β ( $n=5$ ). **g** Summary of NKG2A expression on sorted naive CD8 T cells after coculture with autologous CD4 T cells, monocytes or CD4 T cells + monocytes in the presence of SEB with or without TGF-β ( $n=5$ ). All flow analyses were performed after 8 days of culture. **b, d, f, g** Data are from distinct healthy donors. Horizontal lines indicate the mean  $\pm$  SEM. NS= non-significant;  $p$ -values were determined by one-way ANOVA with Tukey's post hoc test (**d, g**) and by paired 2-tailed  $t$  test (**f**).

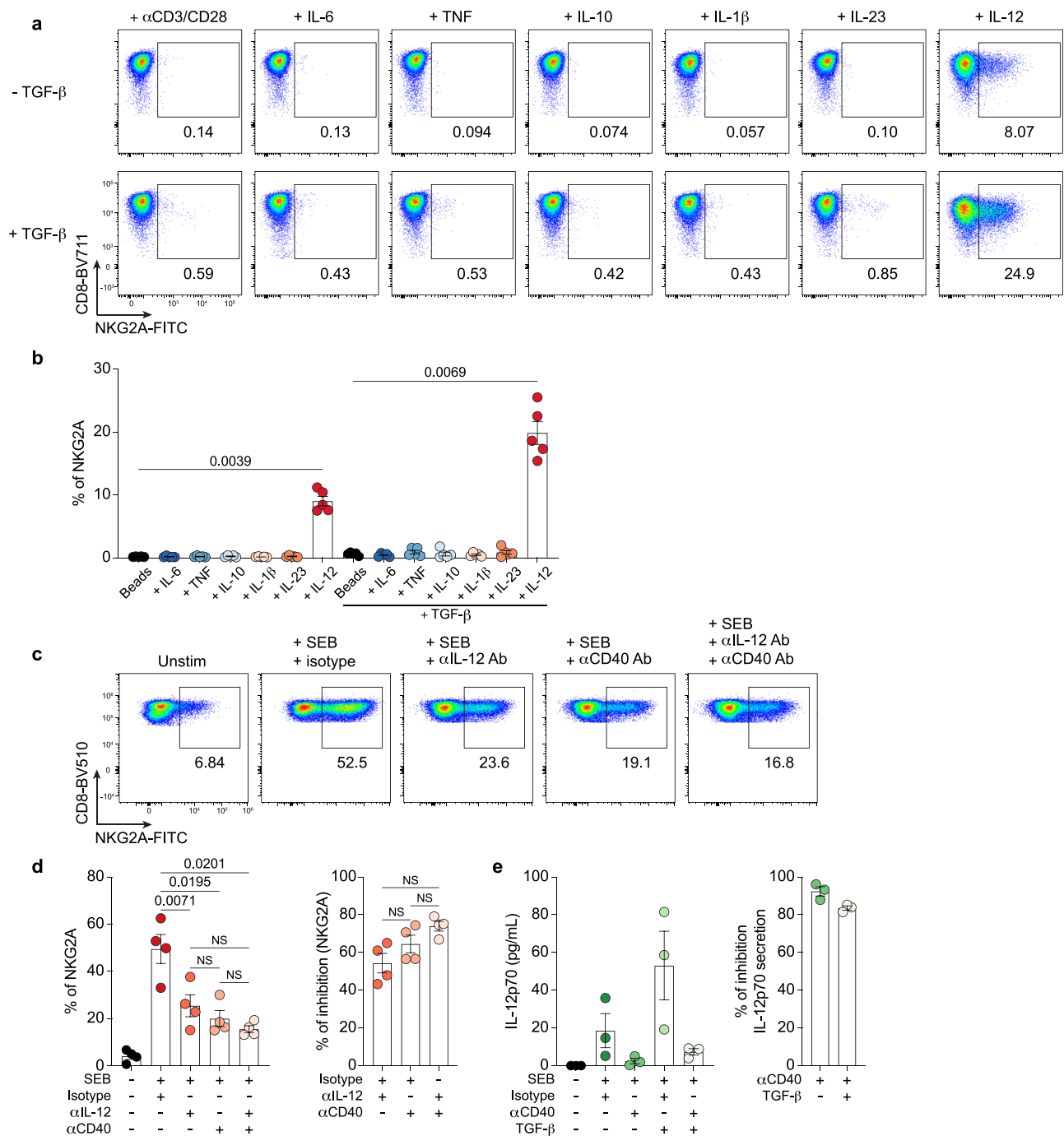


**Fig. 7 | IL-12 plays a central role in the induction of NKG2A on CD8 T cells.** Sorted naïve CD8 T cells were activated with CD3/CD28 beads for 24 hours, rested for 2 days and restimulated with CD3/CD28 beads for 8 days in the presence of the indicated cytokines with or without TGF- $\beta$ . **a** Data from a representative donor and **(b)** summary of NKG2A expression after 8 days of culture are shown ( $n = 5$ ). **c** Expression of NKG2A by CD8 T cells after stimulation of PBMC with SEB in the presence of isotype control,  $\alpha$ -IL-12p70 Ab,  $\alpha$ -CD40 Ab or both. Data from one

representative donor are shown. **d** Summary of **(c)** (left) and percentage inhibition of NKG2A expression by CD8 T cells in the different culture conditions (right) ( $n = 4$ ). **e** Detection of IL-12p70 in the culture supernatants of PBMCs stimulated for 3 days with SEB in presence or not of  $\alpha$ -CD40 Ab (left) and percentage inhibition of IL-12p70 secretion (right) ( $n = 3$ ). **b**, **d**, **e** Data are from distinct healthy donors. Horizontal lines indicate the mean  $\pm$  SEM. NS= non-significant;  $p$ -values were determined by one-way ANOVA with Tukey's post hoc test (**b**, **d**, **e**).

thereby restore or improve tumor cell killing. Of note, the proportion of NKG2A<sup>+</sup> cells among DP CD8 TILs varied between patients, suggesting that selection of patients with high frequencies of NKG2A<sup>+</sup> cells might improve outcome for NKG2A blockade in cancer patients. Interestingly, phenotypic analysis revealed that HPV<sup>+</sup> HNSCC tumors have a low frequency of NKG2A<sup>+</sup> cells within DP CD8 TILs, which could limit the impact of NKG2A blockade in this patient group. The difference in NKG2A expression by DP CD8 TILs in HPV<sup>-</sup> and HPV<sup>+</sup> HNSCC

tumors might be linked to differences in the immune cell composition in the TME<sup>45</sup>, resulting in unique secretome patterns. However, future studies would need to be performed to validate this hypothesis.

Another important aspect of our work relates to the stability of NKG2A on CD8 T cells. We observed that following in vitro polyclonal T-cell expansion the majority of NKG2A<sup>+</sup> DP CD8 TILs maintained NKG2A expression. This is not unique to CD8 T cells as the stability of NKG2A expression had also been demonstrated on  $\gamma\delta$  T cells<sup>24</sup>. The

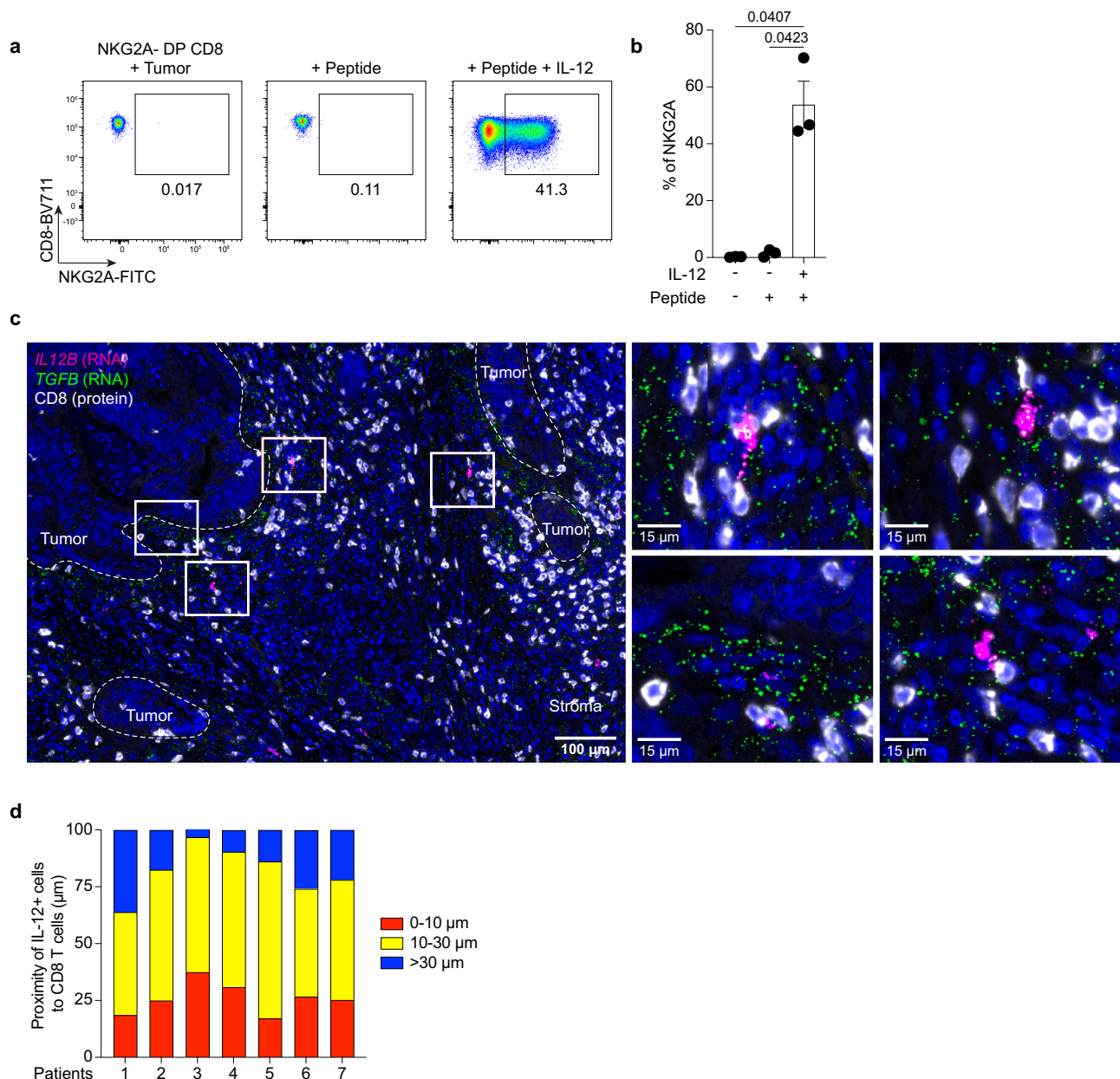


**Fig. 8 | IL-12 induces NKG2A expression on tumor-reactive CD8 T cells and is secreted in the TME.** **a** Flow cytometry analysis and **(b)** summary of the induction of NKG2A expression by NKG2A<sup>+</sup> DP CD8 TILs cultivated for 8 days with an HLA-matched tumor cell line pulsed with their cognate peptide in presence or absence of IL-12 ( $n = 3$ ). **c** ISH/IF for IL12 (RNA, magenta), TGF- $\beta$  (RNA, green) and CD8 (protein, white). Representative low-power image of a CRC tumor sample (left), together with high-power views of four selected areas (right) are shown. Scale

bar = 100  $\mu$ m for the low-power image and 15  $\mu$ m for high-power views. **d** The graph illustrates the distance (in  $\mu$ m) of IL-12<sup>+</sup> cells to CD8 T cells. The proportion of IL-12<sup>+</sup> cells within 0–10  $\mu$ m, 10–30  $\mu$ m and > 30  $\mu$ m is indicated. The analysis was performed on the tumor from 7 patients (3 HNSCC and 4 CRC). **g**, Data are from tumor-reactive CD8 T cell lines isolated from three cancer patients. Horizontal lines indicate the mean  $\pm$  SEM. NS = non-significant;  $p$ -values were determined by one-way ANOVA with Tukey's post hoc test.

stable expression of this inhibitory receptor on tumor-reactive CD8 T cells could affect their cytotoxic function<sup>12,14</sup> and reduce the efficacy of adoptive T cell therapy should tumor cells express high levels of HLA-E. To overcome this barrier, one might consider knocking down NKG2A expression prior to adoptive transfer using a lentiviral or a CRISPR approach. Another strategy would be to combine adoptive T cell therapy with NKG2A blockade. Of course, NKG2A is only one of many inhibitory receptors expressed by DP CD8 TILs and unleashing their full potential might require targeting multiple pathways.

Analysis of the TCR repertoire of NKG2A<sup>+</sup> and NKG2A<sup>+</sup> DP CD8 TILs revealed a high level of shared TCR $\beta$  clonotypes, demonstrating a common origin of the two subsets. Furthermore, single cell gene

expression and trajectory analysis suggest that upregulation of NKG2A on CD8 TILs occurs as they develop into DP CD8 T cells. Together, these results indicate that signals present in the TME can influence the development of tumor-reactive T cells, resulting in phenotypic differences that can affect their function. Such differences might reflect a degree of heterogeneity in the TME and the presence of distinct niches. Identification of those niches and analysis of the spatial distribution of tumor-reactive T cells within the TME might provide new strategies to treat cancer patients.

In contrast with previous studies, we found that TCR activation and TGF- $\beta$  were not sufficient to induce NKG2A expression by naïve CD8 T cells<sup>39,40</sup>, which suggested that other signals were required.

Among the multiple cytokines tested, only IL-12 was able to induce NKG2A expression on naïve CD8 T cells in conjunction with TCR stimulation. Our results are in accordance with previous studies showing a role for IL-12 in increasing NKG2A expression on human NK cells<sup>46,47</sup> and CD8 T cells<sup>48</sup>, and further support a central role for IL-12 in that process. Our work established that NKG2A upregulation in response to SEB depends on CD4 T cells and APCs. More precisely, we found that IL-12 secretion by APCs, which is potentiated by the CD40/CD40L pathway, participated in NKG2A expression. The effect of IL-12 on NKG2A expression was also demonstrated on NKG2A<sup>+</sup> DP CD8 T cells isolated from tumors. Analysis of the TME revealed that only a small number of cells in the TME produce IL-12 and those cells are located near the invasive margin of the tumor where CD8 T cells are present. These cells might correspond to the population of IL-12-producing dendritic cells identified by Garriss et al. in a mouse model of CRC<sup>49</sup> but their identity will need to be confirmed in future experiments.

IL-12 is a proinflammatory cytokine known to promote Th1 responses and CD8 T cell differentiation into cytotoxic effector cells which are essential to clear viral infections<sup>50–52</sup> and induce tumor regression<sup>53,54</sup>. For this reason, IL-12 delivery to the tumor to boost the anti-tumor immune response while avoiding systemic toxicity is an active field of research. However, our data suggest that, in addition to its key role as promoter of cytotoxic immune responses, IL-12 can also induce the expression of immunoregulatory molecules that could negatively impact the response. Indeed, we showed that IL-12 induces NKG2A expression on CD8 T cells but also increases the expression of CD39, an ectonucleotidase that participates in the degradation of ATP into adenosine, a potent immunosuppressive metabolite<sup>55</sup>. Induction of those molecules by IL-12 might participate in a negative feedback loop to prevent overactivation of the immune system but can antagonize the anti-tumor immune response in cancer patients. Therefore, future studies will need to carefully examine the effects of IL-12 on the phenotype and function of the effectors of the anti-tumor immune response and its use in patients might require combination with immune checkpoint blockade.

## Methods

### Blood and tumor samples

Peripheral blood, and tumor samples were obtained from individuals diagnosed with HNSCC and mismatch-repair proficient colorectal cancers (MMR-p CRC). Peripheral blood was also obtained from healthy donors. All patients and healthy donors signed written informed consent approved by the Providence St. Joseph Institutional Review Board (IRB protocol nO. 06-108 A) and the study was conducted in accordance with the ethical standards established by the Declaration of Helsinki. At the time of sample collection, patients were not undergoing therapy. Previously, they may have undergone a wide range of therapies, including chemotherapy, radiotherapy, surgery, and immunotherapy, or none of the above.

Peripheral blood mononuclear cells (PBMC) were purified from whole blood over Ficoll-Paque PLUS (GE Healthcare) gradient and cryopreserved prior to analysis. Tumor samples were prepared under sterile conditions, cut into small pieces, and digested in RPMI-1640 medium in the presence of hyaluronidase at 0.5 mg/ml (Sigma-Aldrich, cat#H6254), collagenase at 1 mg/ml (Sigma-Aldrich, cat#C5138) and DNase at 30U/ml (Roche, cat#04536282001) and human serum albumin (MP Biomedicals, cat #IC08823051) at 1.5% final concentration. Cells were digested for 1 hour at RT under agitation with a magnetic stir bar. Cell suspensions were filtered through a 70µm filter. Tumor single-cell suspensions were cryopreserved until further analysis.

### Flow cytometry analysis

After thawing, cryopreserved tumor digests and PBMCs were incubated with a fixable live/dead dye to distinguish viable cells (BioLegend, Zombie Yellow Fixable Viability kit, cat #423104) before staining

with a combination of antibodies (Supplementary Table 1). Cell surface staining was performed in FACS buffer. Intracellular staining was performed using the Fix/Perm kit from eBioscience according to the manufacturer's instructions. Stained cells were acquired either on a LSRII and LSRII Fortessa flow cytometer (BD Biosciences) or a Cytex Aurora from Cytex Biosciences. Data were analyzed with FlowJo software 10.7.1 (Treestar).

### CITE-Seq and single cell RNA-sequencing (scRNA-seq)

Cryopreserved tumor-infiltrating lymphocytes (TILs) were thawed and enriched for immune cells using CD45 (TIL) MicroBeads (Miltenyi Biotec) following the manufacturer's protocol. After enrichment, cells were stained with a mix of fluorescent antibodies (CD45 BV510, #368526, clone 2D1, and CD3 FITC, cat #300440, clone UCHT1) and TotalSeq-C antibodies (CD4, cat #344651 clone SK3; CD8, cat #344753 clone SK1; CD39, cat #328237 clone A1; CD103, cat #350233 clone Ber-ACT8; CD127, cat#351356 clone A019D5; CD25, cat#302649 clone BC96; PD-1, cat#329963, clone EH12.2H7; ICOS, cat#313553 clone C398.4 A) all from BioLegend. To exclude dead cells, propidium iodide (PI) was added just before sorting. Cells were sorted on a FACS Aria II (BD Biosciences) as PI<sup>CD45</sup> CD3<sup>+</sup> into an eppendorf tube. After the sort, samples were prepared according to the Chromium Next GEM Single Cell 5' kit protocol (10x Genomics). The libraries were sequenced on a NovaSeq sequencer from Illumina.

### CITE-seq data processing and clustering

Data were processed with 10X Genomics Cell Ranger (7.0.1 for all HNSCC samples and CRC 4202 samples; 6.1.2 for all other CRC samples) using the human reference genome GRCh38-2020-A. The 'cellranger count' command with the include\_introns=false flag was used to create RNA count matrices and the 'cellranger vdj' command was used to create TCR data for downstream analyzes. Cellranger filtered RNA and ADT count matrices were imported into R (v4.2.2) via Seurat (v4.3.0)<sup>56</sup>. Then, the DSB R package (v1.0.3)<sup>57</sup> was used to normalize the protein matrices via the DSBNormalizeProtein command. Background drops were identified as those with between 0–10<sup>2.5</sup> ADT counts as well as less than 400 unique genes. Singlets were identified as those with more than 10<sup>2.25</sup> ADT count, unique genes between 400 and 6000, less than 15,000 total RNA count, and less than 5% of the counts mapping to mitochondrial genes. RNA data were normalized via Seurat's NormalizeData function with default parameters. CD8 + CD4<sup>+</sup> cells were selected based on CD8 and CD4 density plots. Following CD8 + CD4<sup>+</sup> selection, CD8 subgroups were labeled based on CD39 and CD103 density plots.

To cluster the cells, a gene blacklist containing TCR genes, cell-cycle genes, and mitochondrial genes was first created and used to filter any variable gene list. Then, the 'CellCycleScoring' function was used to determine S and G2M scores as well as cell phases. Scaled residuals of RNA count data were generated by regressing out the effects of cell-cycle scores, percent mitochondrial counts, and UMI counts per cell. PCA was run and the PCs were then harmonized using 'RunHarmony' function of the harmony R package (v0.1.1)<sup>58</sup>. For ADT, all ADTs were scaled using 'ScaleData', PCA was run on the scaled ADTs and then harmonized. Weighted Nearest Neighbors (WNN) were then determined via the 'FindMultiModalNeighbors' command using the first 20 RNA harmonized PCs and all 7 of the ADT harmonized PCs. The resulting shared nearest neighbor graph was then used as input into Seurat's 'FindClusters' function at a resolution of 0.4 (0.3 for CRC clustering) and the 'RunUMAP' function with n.neighbors = 20.

### Trajectory inference

Prior to trajectory inference it is important to filter the cells so all populations likely contain a common progenitor within the same dataset to avoid forcing a trajectory that may not be real. Additionally, since harmonizing the data only affects PCs, and integrated gene



expression data were needed to create diffusion maps, an additional method was used to integrate and scale the RNA data.

First, MAIT cells (identified as cells with “TRAV1-2.TRAJ33” TCR in the cellranger v2 output) were removed from the Seurat object. Then, the RNA data were integrated using the Seurat CCA method. The CCA method entailed splitting the Seurat object by sample into a list of sample-level objects. Each object was then normalized (default settings), the most overlapping variable genes between objects were identified and filtered to remove blacklisted genes, and the remaining genes were used to integrate the datasets. The integrated dataset was then scaled while regressing cell-cycle scores, percent mitochondrial counts, and number of UMIs per cell. The scaled data were then used to run PCA, create a nearest neighbor graph using the top 20 PCs, find clusters at a resolution of 1, and generate a UMAP using the top 20 PCs. This integrated object then underwent different gene expression analysis by finding markers for each cluster via the ‘FindAllMarkers’ function restricting the search space so that a gene must be present in at least 30% of cells in a cluster to be tested. The resulting markers were subset to those with an adjusted *p*-value less than 0.05. The top 20 average log2 fold-change markers for each cluster were included into a custom heatmap plot. The resulting heatmap, percent mitochondrial counts violin plot, and number of RNA UMIs per cell violin plot were used to filter out any RNA-based clusters that were not appropriate for trajectory inference such as a small proliferative cell cluster, *FOXP3*+ cluster, and a low-quality cell cluster. HNSCC dataset also had a small likely blood-derived CD8 terminal effector T-cell cluster (*FGFBP2* + *FCGR3A*+) filtered and the CRC dataset had a MAIT cell cluster (*KLRB1* + *RORA*+) filtered as well.

After filtering, the integrated scaled data were used as input to the ‘DiffusionMap’ function of destiny R package (v3.10.0). Finally, the remaining cells of the RNA-integrated Seurat object were then used to filter the original WNN Seurat object in preparation for CellRank. The resulting Seurat object will be referred to as the trajectory-filtered object. The trajectory-filtered object had its metadata, RNA counts matrix, harmony embeddings, diffusion map, and WNN connectivities matrix saved into CellRank. Finally, spliced and unspliced gene count matrices were created via STAR<sup>59</sup> in STARsolo mode.

CellRank v2.0.0 was used as the main package for trajectory inference. Briefly, the above components of the trajectory-filtered Seurat object were imported into Python and used to create an AnnData object. Then, the spliced and unspliced matrices were imported, processed to align the features and cell barcodes, and incorporated into layers within the AnnData object. Then, RNA velocity was calculated via scVelo<sup>60</sup> using the dynamic method.

The velocity graph was then used to create a VelocityKernel which was combined with a ConnectivityKernel using the weighted nearest neighbor connectivities matrix in place of the default connectivities using the conn\_key parameter. The combined kernel is weighted 80% towards the VelocityKernel and 20% towards the ConnectivitiesKernel. This combined kernel was used as input into the Generalized Perron Cluster Cluster Analysis (GPCCA) estimator via the cellrank.estimators.GPCCA function. This estimator (g) was then used to calculate macrostates and fate probabilities. 5 HNSCC macrostates were calculated based on the presence of a known macrostate as well as allowing the algorithm to choose between 5, 6 or 7 macrostates. 6 CRC macrostates were calculated similarly. The initial state was determined via naïve marker enrichment and the terminal states were all other macrostates for HNSCC and all others excluding one very similar to macrostate 3 for CRC. The fate probabilities of each cell to each terminal state was calculated via g.compute\_fate\_probabilities and circular plots were created via cellrank.pl.circular\_projection. To calculate latent time, a starting cell was designated by using Scanpy<sup>61</sup> to create a diffusion map and selecting the tip of one branch with the initial macrostate present and then running scvelo.tl.latent\_time. To create gene smoothers over latent time, we created a model using cellrank.models.GAMR(AnnDataObject,

n\_knots=6, distribution=‘gaussian’). This model was then used to plot gene trends over latent time via cellrank.pl.gene\_trends and the heatmap over latent time via cellrank.pl.heatmap along with first-order moments as the imputed value visualized.

### Expansion of CD8 T cells from the blood and the tumor

Cryopreserved tumor and PBMC samples were thawed and labeled for sorting. Tumor samples were enriched for immune cells using CD45 (TIL) MicroBeads (Miltenyi Biotec) following the manufacturer’s protocol. The enriched fractions were then labeled, and cell populations of interest were sorted on a BD FACSAria II. From PBMCs, naïve CD8<sup>+</sup> T cells were sorted as CD45<sup>+</sup> CD4<sup>+</sup> CD8<sup>+</sup> CD45RA<sup>+</sup> CCR7<sup>+</sup> and memory CD8 T cells as CD45<sup>+</sup> CD4<sup>+</sup> CD8<sup>+</sup> CD45RA<sup>+</sup> CCR7<sup>+</sup> and CD45RA<sup>+</sup> CCR7<sup>+</sup>. From tumor, CD8 T cell subsets were sorted as CD45<sup>+</sup> CD4<sup>+</sup> CD8<sup>+</sup> CD45RA<sup>+</sup> CCR7<sup>+</sup> CD39<sup>+</sup> CD103<sup>+</sup> (double negative CD8, DN CD8), CD39<sup>+</sup> CD103<sup>+</sup> (single positive CD8, SP CD8) CD39<sup>+</sup> CD103<sup>+</sup> NKG2A<sup>+</sup> (double positive CD8 NKG2A<sup>+</sup>, NKG2A<sup>+</sup> DP CD8) and CD39<sup>+</sup> CD103<sup>+</sup> NKG2A<sup>+</sup> (double positive CD8 NKG2A<sup>+</sup>, NKG2A<sup>+</sup> DP CD8). Sorted T cells (1,000 – 2,500 cells/well) were stimulated polyclonally in a 96-well U-bottom plate (Corning/Costar, cat #4401) with 1 µg/ml Phytohemagglutinin (PHA) (Remel, cat #R30852801) in the presence of irradiated (5,000 rad) allogeneic feeder cells (PBMC; 2 × 10<sup>5</sup> cells per well) and 10 ng/ml of recombinant human IL-15 (BioLegend, cat #570304). Cells were cultured in complete RPMI-1640, supplemented with 2 mmol/L L-Glutamine (Gibco, cat #25030081), 1% (vol/vol) nonessential amino acids (Gibco, cat #11140050), 1% (vol/vol) sodium pyruvate (Gibco, cat #11360070), penicillin (50 U/ml) + streptomycin (50 µg/ml) (Gibco, cat #15140122), 10 µg/ml Gentamicin (Thermo Fisher Scientific, cat #15750-060), and 10% pooled human serum (in house preparation). T-cell lines were split when wells reached confluency and lines were maintained in complete medium with IL-15 until analysis or cryopreserved in liquid nitrogen.

For TCR sequencing analysis, DNA extraction was performed on the sorted fraction.

### DNA extraction and TCR-sequencing

Deep sequencing of the variable V-J or V-D-J regions of TCRβ genes was performed on genomic DNA of sorted T cell populations. DNA was extracted from ex vivo sorted CD8 T cell subsets (DNeasy Blood and Tissue Kit, cat #69504, Qiagen). The TCRβ CDR3 regions were sequenced and mapped using the human hsTCRB sequencing kit (ImmunoSEQ, cat #ISK10101, Adaptive Biotech). Samples were sequenced using a MiSeq sequencer (Illumina). Coverage per sample was > 10x. Only data from productive rearrangements were extracted from the ImmunoSEQ Analyzer platform for further analysis. The circos plots were created with the circlize R package<sup>62</sup> and depict TCR repertoire similarity between different populations of cells. The ribbons connect a highlighted population with other populations that contain shared productive nucleotide sequences. Connections between the non-highlighted populations are not depicted. The width of the ribbon at each end is the proportion of total sequences in that population that are shared with the connected population. To compare the TCR Vβ overlap (or similarity) of two given populations, we used the Morisita’s overlap index.

### Whole-exome and RNA sequencing

Genomic DNA and total RNA were purified from 5 µm FFPE tumor sections on an automated QiaCube instrument using DNA/RNA AllPrep reagents (Qiagen) according to the manufacturer’s instructions. Corresponding normal DNA for germline exome testing was purified from the matching patient’s in vitro expanded T cells or PBMCs as above. DNA and RNA were quantified using a Qubit fluorometer (Thermo-Fisher). WES for tumor and germline specimens was performed on purified DNA as follows: DNA was prepared into tagged sequencing libraries using Kapa HyperPlus library preparation reagents (Roche)

and exome hybrid-capture was performed using the xGen Research Panel kit (IDT). Captured library pools were normalized and loaded onto a HiSeq 4000 sequencer (Illumina) for next-generation sequencing. WES reads were aligned to Genome Reference Consortium Human Build 37 (hg19) followed by GATK preprocessing. Four independent single nucleotide mutation callers (Varscan 2.3.6, SomaticSniper 1.0.5.0, Mutect 1.1.7 and Strelka 1.0.15) were used to call somatic nonsynonymous single nucleotide variants and two Insertion-Deletion callers (Strelka 1.0.15 and Varscan 2.3.6) were used to identify somatic nonsynonymous indels. Identified mutations were filtered according to the following criteria: minimum coverage of 10 reads, greater than 5% variant allele frequency (VAF) and called by 2 or more callers. Somatic mutations that passed the filters were further annotated with 1000 genomes project, Exome Aggregation Consortium (ExAC), The Catalog of Somatic Mutations in Cancer

(COSMIC) databases using Annovar. SNPeff was used to predict variant functional effect. An mRNA sequencing library was also prepared from FFPE tissues using RNA Access Library Preparation reagents (Illumina) according to the manufacturer's instructions. Libraries were pooled and sequenced at a depth of 25–50 million reads on a HiSeq 4000 sequencer (Illumina). RNA alignment was performed using STAR, followed by GATK pre-processing best practices workflow. Fragments per kb per million mapped reads (FPKM) values were calculated using Cufflinks. FPKM levels were used to assess expression of candidate mutations.

### Human papillomavirus (HPV)-specific gene production

To screen for recognition of HPV tumor antigens, four constructs were used, encoding for the full-length amino acid sequences of HPV16 E2, E5, E6 and E7 oncoproteins (367, 83, 159, 99 aa, respectively). The sequences were cloned into pcDNA3.1+CEF-MHC-1-v2 (kindly provided by Dr. Eric Tran) using HindIII and BamHI restriction sites and flanked with AAGCTTGCCACC (5') and GGATCC (3') using GenScript services. After bacteria transformation, plasmid constructs were purified with the Zippy Plasmid Purification Kit (Zymo Research, cat #D4036) and 5 µg of plasmid was digested by the restriction enzyme NotI (New England Biolabs, cat #R3189S). Following linearization of the constructs, DNA was cleaned up using the DNA Clean & Concentrator-5 kit (Zymo Research, cat #D4013). Next, we used 1 µg of linearized DNA to generate in vitro-transcribed (IVT) RNA using the Mmessage Mmachine T7 Ultra kit (Life Technologies, cat #AMB13455) as instructed by the manufacturer. RNA was cleaned up (Zymo Research, cat. #R1017) and concentration was measured using a NanoDrop spectrophotometer prior to use in transfections.

### Tandem minigene (TMG) construction

TMGs were constructed as previously described<sup>63,64</sup>. For each non-synonymous variant identified by WES, we constructed a “minigene”, consisting of the mutant amino acid flanked by 12 amino acids of the wild-type (WT) protein sequence. Up to 16 minigenes were concatenated to generate a tandem minigene (TMG) construct. TMG constructs were codon optimized and subcloned into pcDNA3.1+CEF-MHC-1-v2 (performed by GenScript). The pcDNA3.1+CEF-MHC-1-v2 vector is based on the pcDNA3.1 vector (Thermo Fisher Scientific, cat. #V79020) modified to contain a repeat of the beta-globin 3' UTR sequence and polyA tail after the TMG sequence. These modifications have been found to stabilize in vitro-transcribed RNA<sup>65</sup>. Following the same approach as for the HPV constructs, 1 µg of linearized plasmid DNA was used as a template to generate IVT TMG RNA. RNA was cleaned up (Zymo Research, cat. #R1017) and concentration was measured using a NanoDrop spectrophotometer prior to use in transfections.

### Transfection of HPV RNA or TMG RNA

Cryopreserved autologous expanded memory CD8 T cells were used as APCs for the reactivity experiments. APCs were labeled with Cell

Proliferation Dye eFluor 450 (eBioscience, cat #65084285), washed and resuspended in Opti-MEM (Life Technologies, cat #31985062) at  $20 \times 10^6$  cells/ml. HPV RNA or TMG RNA (4 µg) was added to a 2 mm gap electroporation cuvette (BTX 45-0125, Cole-Parmer), followed by 50 µl of APCs. Cells were electroporated at 250 V for 5 ms for one pulse using a BTX ECM 830 Square Wave Electroporation System (Harvard Bioscience Inc.). Electroporated cells were incubated for 4 hours before coculture with CD8 T cell subsets.

### Peptide synthesis and peptide pulsing

To identify the HPV peptides recognized, we used an overlapping peptide library, encoding for the full-length amino acid sequences of the HPV16 E6 oncoprotein. The 15 mer peptides overlapped by 11 amino acids. HPV16 E6 contained 37 peptides. Peptides were synthesized by Genscript. For the identification of neoantigens, the sequences of the tumor-specific somatic mutations contained in the TMG(s) recognized by CD8 TILs were converted in FASTA format and ran through the NetMHCpan 4.0 Server (Technical University of Denmark). NetMHCpan generates 8 mer to 11 mer peptides from the 25 mer putative neoantigen sequences and predicts binding affinity to patient-specific MHC class I molecules. Peptides with a percentage rank below 2 were considered candidates for further evaluation. Those peptides were synthesized by Genscript and subsequently tested for reactivity against patient's DP CD8 TILs.

### Flow cytometry to assess T-cell recognition of antigens

The reactivity of predicted neoepitopes and HPV antigens against sorted and in vitro expanded CD8 + T cell populations was assessed by flow cytometry (4-1BB up-regulation). T cells were typically thawed and rested for two days at 37 °C in complete medium with IL-15 (10 ng/ml). All cocultures were performed in the absence of exogenous cytokines. Electroporated APCs (HPV RNA) or peptide-pulsed APCs were incubated with T cells ( $1 \times 10^5$  T cells/well) and incubated at 37 °C. Plate-bound anti-CD3 antibody (OKT3, BioLegend, cat # 317326, 1 µg/ml) was used as positive control. 4-1BB up-regulation was assessed after 18 to 20 hours of coculture. Cells were pelleted, washed with PBS and stained with a fixable live/dead dye to distinguish viable cells (BioLegend, Zombie Yellow Fixable Viability kit) for 8 min at +4 °C in the dark. Cells were washed twice and then stained with the appropriate antibodies (Supplementary Table 1) diluted in FACS buffer for 20 min at +4 °C in the dark. Cells were washed twice with FACS buffer prior to acquisition on a BD LSRII flow cytometer. Data were analyzed with FlowJo software 10.7.1 (Treestar).

### NKG2A induction on total PBMC

PBMC from healthy donor (HD) were thawed and resuspended in complete RPMI-1640, supplemented with 2 mmol/L L-Glutamine (Gibco, cat #25030081), 1% (vol/vol) nonessential amino acids (Gibco, cat #11140050), 1% (vol/vol) sodium pyruvate (Gibco, cat #11360070), penicillin (50 U/ml) + streptomycin (50 µg/ml) (Gibco, cat #15140122), 10 µg/ml Gentamicin (Thermo Fisher Scientific, cat #15750-060), and 10% Fetal Bovine Serum (Peak Serum, cat#PS-FB2).  $1 \times 10^5$  PBMCs per well were plated in a 96-well U-bottom plate (Corning/Costar, cat #4401) and the cells were activated with either 1 µg/ml of Phytohemagglutinin (PHA) (Remel, cat #R30852801), 1 µg/ml of Staphylococcal Enterotoxin B (Fisher Scientific, cat #NC9442400) or Cytostim (Miltenyi Biotec, cat #130092172) for 8 days in presence or absence of TGF-β (BioLegend, cat #781802). At day 4 and day 6, half of the medium was replaced with medium supplemented with IL-2 (Prometheus) at 50 U/ml final. At day 8 the cells were analyzed for NKG2A expression and activation status by flow cytometry (For antibody panel details, see Supplementary Table 1).

Depletion of CD4 T cells from PBMC was performed using the CD4 MicroBeads from Miltenyi Biotec (cat # 130-045-101) following the manufacturer instructions.  $1 \times 10^5$  CD4-depleted PBMC (PBMC ΔCD4)

per well were plated in presence of SEB and cultured as described above. At day 8, the expression of NKG2A was analyzed by flow cytometry.

### Upregulation of NKG2A on sorted naïve CD8 T cells

PBMC from HD were thawed and washed once with wash buffer. CD8 enrichment was performed using the CD8 MicroBeads from Miltenyi Biotec (cat # 130-045-201) following the manufacturer instructions. The positive fraction was washed with PBS then stained for 8 min at +4 °C with fixable live/dead dye (BioLegend, Zombie Yellow Fixable Viability kit, cat #423104) to distinguish viable cells. Cells were then washed and stained with a cocktail of fluorescent antibodies (Supplementary Table 1) for 20 min at +4 °C. Naïve CD8 T cells were sorted as CD4<sup>+</sup> CD8<sup>+</sup> CCR7<sup>+</sup> CD45RA<sup>+</sup> NKG2A<sup>+</sup>. Populations of interest were sorted on a FACS Aria II (BD). After sort 50,000 naïve CD8 T cells were plated in a 96-well U-bottom plate (Corning/Costar, cat #4401) together with Dynabeads Human T-Activator CD3/CD28 (Thermo Fisher Scientific, cat #11131D) (1 bead for 5 T cells) in the presence or absence of TGF- $\beta$  (BioLegend, cat #781802). At day 4 and day 6, half of the medium was replaced with medium supplemented with IL-2 (Prometheus) at 50 U/ml final. At day 8 the cells were analyzed for NKG2A expression and activation status by flow cytometry (For antibody panel details, see Supplementary Table 1).

For naïve CD8 T cell restimulation, beads were removed after 24 hours of culture using a magnetic plate and IL-2 at 20 U/ml was added to each well. After two days, CD8 T cells were harvested, counted and 50,000 CD8 T cells per well were plated in a 96-well U-bottom plate in presence of Dynabeads Human T-Activator CD3/CD28 (Thermo Fisher Scientific, cat #11131D) (1 bead for 10 T cells) in the presence of IL-2 (50 U/ml) and different cytokine combinations (BioLegend): IL-6 (cat #570802, 10 ng/ml), TNF (cat #570102, 10 ng/ml), IL-10 (cat #571002, 10 ng/ml) IL-1 $\beta$  (cat #579404, 10 ng/ml), IL-23 (cat #574102, 10 ng/ml), IL-12 (cat #573002, 10 ng/ml), TGF- $\beta$ , 1 ng/ml). Cells were kept in culture and analyzed after 8 days of restimulation (For antibody panel details, see Supplementary Table 1).

For coculture experiment of naïve CD8, conventional CD4 T cells (CD4 Tconv) and monocytes, CD14<sup>+</sup> enrichment using the CD14 MicroBeads from Miltenyi Biotec (cat # 130-050-201) was performed prior to CD8 enrichment. The CD14<sup>+</sup> fraction was kept on ice in complete RPMI-1640 supplemented with 10% FBS. The CD14<sup>+</sup> fraction was used to enrich CD8 T cells using the CD8 MicroBeads from Miltenyi Biotec (cat # 130-045-201). The CD8<sup>+</sup> and CD8<sup>-</sup> fractions were washed with PBS and stained separately for 8 min at +4 °C with fixable live/dead dye to distinguish viable cells (BioLegend, Zombie Yellow Fixable Viability kit, cat #423104). The cells were then washed and stained with 2 different combinations of antibodies (Supplementary Table 1) for 20 min at +4 °C in the dark. From the CD8<sup>+</sup> fraction, naïve CD8 T cells were sorted as described above. From the CD8<sup>-</sup> fraction, CD4 Tconv were sorted as CD4<sup>+</sup> CD8<sup>-</sup> CD127<sup>+</sup>/CD25<sup>low</sup> to exclude regulatory T cells. Populations of interest were sorted on a FACS Aria II (BD). After sort, populations were counted and resuspended in complete RPMI-1640 supplemented with 10% FBS. Experiments were performed using 25,000 CD14<sup>+</sup>; 50,000 CD4 Tconv and 25,000 naïve CD8 T cells in 96-well U-bottom plate (Corning/Costar, cat #4401). Cells were activated, cultivated, and analyzed for NKG2A upregulation by flow cytometry (For antibody panel details, see Supplementary Table 1).

For IL-12p70 and CD40L blocking experiments, anti-Human IL-12p70 (R&D Systems, cat #MAB219-100, 10  $\mu$ g/ml final), anti-CD40 (BioLegend, cat #313019, clone HB14, 10  $\mu$ g/ml final) or isotype control mouse IgG1 (BioLegend, cat #400166, clone MOPC21, 10  $\mu$ g/ml final) were added in the corresponding wells. Cells were cultured and analyzed for NKG2A upregulation by flow cytometry as previously described.

For the IL-12p70 ELISA, supernatants from naïve CD8 T cells, CD4 Tconv and CD14 coculture were harvested at day 3. ELISA was

performed using the BD OptEIA Human IL 12 (p70) ELISA Set (BD, cat #555183) according to manufacturer instructions. Plates were read on the SpectraMax iD3 from Molecular Devices and analyzed with the SoftMaxPro 7 software (version 7.0.3).

### Culture of NKG2A<sup>-</sup> DP CD8 TILs with tumor cells

Tumor antigen-reactive NKG2A<sup>-</sup> DP CD8 TILs identified in Fig. 5 were used for this experiment. Cryopreserved CD8 T cells were thawed and kept in culture for 2 days in complete RPMI-1640 supplemented as described above with 10 ng/ml of IL-15. Human tumor cell lines from HNSCC patients with matching HLA restriction were grown in vitro using complete RPMI-1640 supplemented with 10% FBS. Those cell lines were isolated in Dr. Fox's lab and are not commercially available. After 2 passages, tumor cells were detached using trypsin-EDTA (Thermo Fisher Scientific, cat #25-200-056) and 50,000 tumor cells were plated in a 96-well flat-bottom plate (Cell-treat, cat #229195). Tumor cells were pulsed with the cognate tumor peptides at 5  $\mu$ g/ml and cells were incubated overnight at +37 °C with 5% CO<sub>2</sub>. The following day, tumor cells were washed twice before adding 50,000 NKG2A<sup>-</sup> DP CD8 TILs in the presence or absence of IL-12 (cat #573002, 10 ng/ml final). IL-2 at 50 U/ml was added to all wells. Cells were kept in culture and NKG2A upregulation was assessed by flow cytometry after 8 days (For antibody panel details, see Supplementary Table 1).

### RNAscope

Experiments were performed as detailed in Advanced Cell Diagnostics (ACD) protocol for the RNAscope Multiplex Fluorescent Reagent Kit v2 (ACD, cat #323100) and RNA Protein Co-Detection Ancillary Kit (ACD, cat #3231800). RNA and protein co-detection was performed on formalin-fixed paraffin-embedded (FFPE) human tissue samples obtained from Providence Portland Medical Center Pathology department. Tissue blocks were cut into serial sections at 5  $\mu$ m thickness and placed onto Superfrost Plus Adhesion Slides (Fisher Scientific). Sections were deparaffinized at room temperature using xylene, 100% ethanol, 95% ethanol, 70% ethanol, with a final wash in DI water. After deparaffination, target retrieval was performed using a Hamilton Beach steamer. Following retrieval, immunofluorescence combined with in situ hybridization (ISH) was performed on the tissue sections using 4 RNA target probes and one protein marker according to the manufacturer's protocol. Two experiments were carried out. The first assay evaluated *IL12B* (ACD, Cat #402071) and *TGFB* (ACD, Cat #40881-C3) target probes. The second assay evaluated *KLRC1* (NKG2A) (ACD, Cat #541331), *ENTPDI* (CD39) (ACD, Cat #474181-C2). Both assays used a protein marker for CD8 (Invitrogen, SP16; Cat #MA5-16345SP16). RNA and antigen-antibody binding was visualized with Opal-TSA reagents (Akoya Biosciences). Tissue slides were counterstained with DAPI from ACD and coverslipped with VECTASHIELD antifading mounting media (Vector Labs). Detailed information regarding RNA probes, antibody dilution, TSA-Opal reagents is provided in Supplementary Table 2.

Digital images were acquired with a Vectra 3.0 Automated Quantitative Pathology Imaging System and Phenolmager Fusion instrument (Akoya Biosciences). Whole slide scans were acquired using a 10x objective lens to identify regions of interest (ROIs). Six to fifteen ROIs were selected from each tissue sample for analysis. Inform 3.0 software (Akoya Biosciences) was used to perform cell segmentation and phenotyping of individual cells according to the protein marker and DAPI.

### Statistical analysis

Statistical significance between groups was determined by 1-way ANOVA with Tukey's correction or by unpaired or paired 2-tailed *t* test. For each test, a *P*-value of less than 0.05 was considered statistically significant. Analyses were performed with GraphPad Prism 10 (GraphPad Software).



## Reporting summary

Further information on research design is available in the Nature Portfolio Reporting Summary linked to this article.

## Data availability

TCR-sequencing data have been deposited in the ImmuneACCESS database (Adaptive Biotechnologies), available at <https://clients.adaptivebiotech.com/pub/fesneau-2024-nc> (<https://doi.org/10.21417/OF2024NC>) and are publicly available as of the date of publication. WES and RNA sequencing (RNA-seq) read-level data are not available due to the presence of germline variants in the underlying data. Any inquiries for further access should be directed to our Data Sharing Committee at [eacri.bioinformatics@providence.org](mailto:eacri.bioinformatics@providence.org) and we will grant access to the deidentified data sets for research purposes. Processed, de-identified CITE-seq data generated during this study have been deposited in the Gene Expression Omnibus (GEO) under the accession number [GSE278692](https://www.ncbi.nlm.nih.gov/geo/query/acc.cgi?acc=GSE278692) (<https://www.ncbi.nlm.nih.gov/geo/query/acc.cgi?acc=GSE278692>). All other data are available within the article and its Supplementary files. Source data are provided with this paper.

## References

- Duhen, T. et al. Co-expression of CD39 and CD103 identifies tumor-reactive CD8 T cells in human solid tumors. *Nat. Commun.* **9**, 2724 (2018).
- Simoni, Y. et al. Bystander CD8(+) T cells are abundant and phenotypically distinct in human tumour infiltrates. *Nature* **557**, 575–579 (2018).
- Thommen, D. S. et al. A transcriptionally and functionally distinct PD-1(+) CD8(+) T cell pool with predictive potential in non-small-cell lung cancer treated with PD-1 blockade. *Nat. Med.* **24**, 994–1004 (2018).
- Rajamanickam, V. et al. Robust antitumor immunity in a patient with metastatic colorectal cancer treated with cytotoxic regimens. *Cancer Immunol. Res.* **9**, 602–611 (2021).
- van den Bulk, J. et al. CD103 and CD39 coexpression identifies neoantigen-specific cytotoxic T cells in colorectal cancers with low mutation burden. *J. Immunother. Cancer* **11**, e005887 (2023).
- van Montfoort, N. et al. NKG2A blockade potentiates CD8 T cell immunity induced by cancer vaccines. *Cell* **175**, 1744–1755.e1715 (2018).
- Dahmani, A. & Delisle, J. S. TGF- $\beta$  in T cell biology: implications for cancer immunotherapy. *Cancers (Basel)* **10**, 194 (2018).
- Thomas, D. A. & Massague, J. TGF- $\beta$  directly targets cytotoxic T cell functions during tumor evasion of immune surveillance. *Cancer Cell* **8**, 369–380 (2005).
- Le, D. T. et al. Mismatch repair deficiency predicts response of solid tumors to PD-1 blockade. *Science* **357**, 409–413 (2017).
- Le, D. T. et al. PD-1 Blockade in tumors with mismatch-repair deficiency. *N. Engl. J. Med.* **372**, 2509–2520 (2015).
- Overman, M. J. et al. Nivolumab in patients with metastatic DNA mismatch repair-deficient or microsatellite instability-high colorectal cancer (CheckMate 142): an open-label, multicentre, phase 2 study. *Lancet Oncol.* **18**, 1182–1191 (2017).
- Andre, P. et al. Anti-NKG2A mAb is a checkpoint inhibitor that promotes anti-tumor immunity by unleashing both T and NK Cells. *Cell* **175**, 1731–1743.e1713 (2018).
- Patel, S. P. et al. Phase 1/2 study of monalizumab plus durvalumab in patients with advanced solid tumors. *J. Immunother. Cancer* **12**, e007340 (2024).
- Ducoin, K. et al. Targeting NKG2A to boost anti-tumor CD8 T-cell responses in human colorectal cancer. *Oncoimmunology* **11**, 2046931 (2022).
- Hair, J., Robinson, M. J., Wilkinson, R. W. & Dovedi, S. J. Deep phenotyping of surface stimulatory and inhibitory co-receptors on cancer-resident T and NK cells reveals cell subsets within the tumor-reactive CTL population that are uniquely defined by NKG2A expression. *SLAS Discov.* **27**, 95–106 (2022).
- Braud, V., Aldemir, H., Breart, B. & Ferlin, W. Expression of CD94–NKG2A inhibitory receptor is restricted to a subset of CD8+ T cells. *Trends Immunol.* **24**, 162–164 (2003).
- Borst, L., van der Burg, S. H. & van Hall, T. The NKG2A–HLA-E axis as a novel checkpoint in the tumor microenvironment. *Clin. Cancer Res.* **26**, 5549–5556 (2020).
- Andersson, E. et al. Non-classical HLA-class I expression in serous ovarian carcinoma: correlation with the HLA-genotype, tumor infiltrating immune cells and prognosis. *Oncoimmunology* **5**, e1052213 (2016).
- Eugene, J. et al. The inhibitory receptor CD94/NKG2A on CD8(+) tumor-infiltrating lymphocytes in colorectal cancer: a promising new druggable immune checkpoint in the context of HLA-E/ $\beta$ 2m overexpression. *Mod. Pathol.* **33**, 468–482 (2020).
- Kamiya, T., Seow, S. V., Wong, D., Robinson, M. & Campana, D. Blocking expression of inhibitory receptor NKG2A overcomes tumor resistance to NK cells. *J. Clin. Invest.* **129**, 2094–2106 (2019).
- Andre, P. et al. Differential regulation of killer cell Ig-like receptors and CD94 lectin-like dimers on NK and T lymphocytes from HIV-1-infected individuals. *Eur. J. Immunol.* **29**, 1076–1085 (1999).
- Bertone, S. et al. Transforming growth factor- $\beta$ -induced expression of CD94/NKG2A inhibitory receptors in human T lymphocytes. *Eur. J. Immunol.* **29**, 23–29 (1999).
- Braud, V. M. et al. HLA-E binds to natural killer cell receptors CD94/NKG2A, B and C. *Nature* **391**, 795–799 (1998).
- Cazzetta, V. et al. NKG2A expression identifies a subset of human Vdelta2 T cells exerting the highest antitumor effector functions. *Cell Rep.* **37**, 109871 (2021).
- Cazzetta, V., Depierreux, D., Colucci, F., Mikulak, J. & Mavilio, D. NKG2A Immune checkpoint in Vdelta2 T cells: emerging application in cancer immunotherapy. *Cancers (Basel)* **15**, 1264 (2023).
- Malmberg, K. J. et al. IFN- $\gamma$  protects short-term ovarian carcinoma cell lines from CTL lysis via a CD94/NKG2A-dependent mechanism. *J. Clin. Invest.* **110**, 1515–1523 (2002).
- Mingari, M. C. et al. HLA class I-specific inhibitory receptors in human T lymphocytes: interleukin 15-induced expression of CD94/NKG2A in superantigen- or alloantigen-activated CD8+ T cells. *Proc. Natl Acad. Sci. USA* **95**, 1172–1177 (1998).
- Mueller, S. N. & Mackay, L. K. Tissue-resident memory T cells: local specialists in immune defence. *Nat. Rev. Immunol.* **16**, 79–89 (2016).
- Schenkel, J. M. et al. T cell memory. resident memory CD8 T cells trigger protective innate and adaptive immune responses. *Science* **346**, 98–101 (2014).
- Schenkel, J. M. & Masopust, D. Tissue-resident memory T cells. *Immunity* **41**, 886–897 (2014).
- Djenidi, F. et al. CD8+CD103+ tumor-infiltrating lymphocytes are tumor-specific tissue-resident memory T cells and a prognostic factor for survival in lung cancer patients. *J. Immunol.* **194**, 3475–3486 (2015).
- Komdeur, F. et al. CD103+ intraepithelial T cells in high-grade serous ovarian cancer are phenotypically diverse TCR $\alpha\beta$ + CD8 $\alpha\beta$ + T cells that can be targeted for cancer immunotherapy. *Oncotarget* **7**, 75130–75144 (2016).
- Wang, B. et al. CD103+ tumor infiltrating lymphocytes predict a favorable prognosis in urothelial cell carcinoma of the bladder. *J. Urol.* **194**, 556–562 (2015).
- Webb, J. R., Milne, K., Watson, P., Deleeuw, R. J. & Nelson, B. H. Tumor-infiltrating lymphocytes expressing the tissue resident memory marker CD103 are associated with increased survival in high-grade serous ovarian cancer. *Clin. Cancer Res.* **20**, 434–444 (2014).
- Workel, H. H. et al. CD103 defines intraepithelial CD8+ PD1+ tumour-infiltrating lymphocytes of prognostic significance in endometrial adenocarcinoma. *Eur. J. Cancer* **60**, 1–11 (2016).



36. Tran, E. et al. Immunogenicity of somatic mutations in human gastrointestinal cancers. *Science* **350**, 1387–1390 (2015).
37. Tran, E. et al. T-cell transfer therapy targeting mutant KRAS in cancer. *N. Engl. J. Med.* **375**, 2255–2262 (2016).
38. Wolfl, M. et al. Activation-induced expression of CD137 permits detection, isolation, and expansion of the full repertoire of CD8+ T cells responding to antigen without requiring knowledge of epitope specificities. *Blood* **110**, 201–210 (2007).
39. Bertone, S. et al. Transforming growth factor- $\beta$ -induced expression of CD94/NKG2A inhibitory receptors in human T lymphocytes. *Eur. J. Immunol.* **29**, 23–29 (1999).
40. Gunturi, A., Berg, R. E., Crossley, E., Murray, S. & Forman, J. The role of TCR stimulation and TGF- $\beta$  in controlling the expression of CD94/NKG2A receptors on CD8 T cells. *Eur. J. Immunol.* **35**, 766–775 (2005).
41. Niedergang, F. et al. The Staphylococcus aureus enterotoxin B superantigen induces specific T cell receptor down-regulation by increasing its internalization. *J. Biol. Chem.* **270**, 12839–12845 (1995).
42. Gerhardt, L., Hong, M. M. Y., Yousefi, Y., Figueredo, R. & Maleki Vareki, S. IL-12 and IL-27 promote CD39 expression on CD8+ T cells and differentially regulate the CD39+CD8+ T cell phenotype. *J. Immunol.* **210**, 1598–1606 (2023).
43. Kennedy, M. K. et al. CD40/CD40 ligand interactions are required for T cell-dependent production of interleukin-12 by mouse macrophages. *Eur. J. Immunol.* **26**, 370–378 (1996).
44. Shu, U. et al. Activated T cells induce interleukin-12 production by monocytes via CD40-CD40 ligand interaction. *Eur. J. Immunol.* **25**, 1125–1128 (1995).
45. Cillo, A. R. et al. Immune landscape of viral- and carcinogen-driven head and neck cancer. *Immunity* **52**, 183–199.e189 (2020).
46. Cany, J. et al. Combined IL-15 and IL-12 drives the generation of CD34(+) derived natural killer cells with superior maturation and alloreactivity potential following adoptive transfer. *Oncoimmunology* **4**, e1017701 (2015).
47. Saez-Borderias, A. et al. IL-12-dependent inducible expression of the CD94/NKG2A inhibitory receptor regulates CD94/NKG2C+ NK cell function. *J. Immunol.* **182**, 829–836 (2009).
48. Derre, L. et al. Expression of CD94/NKG2-A on human T lymphocytes is induced by IL-12: implications for adoptive immunotherapy. *J. Immunol.* **168**, 4864–4870 (2002).
49. Garriss, C. S. et al. Successful anti-PD-1 cancer immunotherapy requires T cell-dendritic cell crosstalk involving the cytokines IFN- $\gamma$  and IL-12. *Immunity* **49**, 1148–1161.e1147 (2018).
50. Henry, C. J., Ornelles, D. A., Mitchell, L. M., Brzoza-Lewis, K. L. & Hiltbold, E. M. IL-12 produced by dendritic cells augments CD8+ T cell activation through the production of the chemokines CCL1 and CCL17. *J. Immunol.* **181**, 8576–8584 (2008).
51. NA, A. R., Balasubramaniam, V. & Yap, W. B. Potential of interleukin (IL)-12 group as antivirals: severe viral disease prevention and management. *Int. J. Mol. Sci.* **24**, 7350 (2023).
52. Schmidt, M. E. & Varga, S. M. Cytokines and CD8 T cell immunity during respiratory syncytial virus infection. *Cytokine* **133**, 154481 (2020).
53. Rubinstein, M. P. et al. Interleukin-12 enhances the function and anti-tumor activity in murine and human CD8(+) T cells. *Cancer Immunol. Immunother.* **64**, 539–549 (2015).
54. Xue, D. et al. A tumor-specific pro-IL-12 activates preexisting cytotoxic T cells to control established tumors. *Sci. Immunol.* **7**, eabi6899 (2022).
55. Antonioli, L., Pacher, P., Vizi, E. S. & Haskó, G. CD39 and CD73 in immunity and inflammation. *Trends Mol. Med.* **19**, 355–367 (2013).
56. Hao, Y. et al. Integrated analysis of multimodal single-cell data. *Cell* **184**, 3573–3587.e3529 (2021).
57. Mulè, M. P., Martins, A. J. & Tsang, J. S. Normalizing and denoising protein expression data from droplet-based single cell profiling. *Nat. Commun.* **13**, 2099 (2022).
58. Korsunsky, I. et al. Fast, sensitive, and accurate integration of single-cell data with Harmony. *Nat. Methods* **16**, 1289–1296 (2019).
59. Dobin, A. et al. STAR: ultrafast universal RNA-seq aligner. *Bioinformatics* **29**, 15–21 (2013).
60. Bergen, V., Lange, M., Peidli, S., Wolf, F. A. & Theis, F. J. Generalizing RNA velocity to transient cell states through dynamical modeling. *Nat. Biotechnol.* **38**, 1408–1414 (2020).
61. Wolf, F. A., Angerer, P. & Theis, F. J. SCANPY: large-scale single-cell gene expression data analysis. *Genome Biol.* **19**, 15 (2018).
62. Gu, Z., Gu, L., Eils, R., Schlesner, M. & Brors, B. Circize implements and enhances circular visualization in R. *Bioinformatics* **30**, 2811–2812 (2014).
63. Lu, Y. C. et al. Efficient identification of mutated cancer antigens recognized by T cells associated with durable tumor regressions. *Clin. Cancer Res* **20**, 3401–3410 (2014).
64. Tran, E. et al. Cancer immunotherapy based on mutation-specific CD4+ T cells in a patient with epithelial cancer. *Science* **344**, 641–645 (2014).
65. Burkly, L. C., Lo, D. & Flavell, R. A. Tolerance in transgenic mice expressing major histocompatibility molecules extrathymically on pancreatic cells. *Science* **248**, 1364–1368 (1990).

## Acknowledgements

We thank Mark Schmidt, Aaron Encisco and Casey Fairbanks for assistance with consenting patients for this study; Dr Walter J. Urba, Dr Eric Tran, Dr Michael Gough and Dr Rebekka Duhon for reviewing the manuscript and discussions; Rogan Rattray, John Welle and Mary Campbell for TCR-seq, WES and RNA-seq performed at the Providence Molecular Genomics Laboratory; Tanisha Christie and Dr. Yoshi Koguchi for discussions and library preparation for CITE-seq; Miranda Gilchrist, Daniel Rose and Dominick Sanders (EACRI Flow Cytometry Core) for excellent technical assistance. This work was supported by the Providence Portland Medical Foundation.

## Author contributions

O.F. and T.D. designed the experiments; O.F., K.S., B.J., and T.D. performed the experiments; KS performed the RNAscope assays; O.F., K.S., B.J., and T.D. analyzed the data; W.R. and V.R. analyzed the CITE-seq data; T.M. and B.F. provided tumor cell lines for the NKG2A up-regulation on CD8 TILs. O.F. and T.D. wrote the manuscript; T.D. initiated the research program and supervised the study.

## Competing interests

The authors declare not competing interests.

## Additional information

**Supplementary information** The online version contains supplementary material available at <https://doi.org/10.1038/s41467-024-54420-w>.

**Correspondence** and requests for materials should be addressed to Thomas Duhon.

**Peer review information** *Nature Communications* thanks Domenico Mavilio, Tao Wang and the other, anonymous, reviewer(s) for their contribution to the peer review of this work. A peer review file is available.

**Reprints and permissions information** is available at <http://www.nature.com/reprints>

**Publisher's note** Springer Nature remains neutral with regard to jurisdictional claims in published maps and institutional affiliations.

**Open Access** This article is licensed under a Creative Commons Attribution-NonCommercial-NoDerivatives 4.0 International License, which permits any non-commercial use, sharing, distribution and reproduction in any medium or format, as long as you give appropriate credit to the original author(s) and the source, provide a link to the Creative Commons licence, and indicate if you modified the licensed material. You do not have permission under this licence to share adapted material derived from this article or parts of it. The images or other third party material in this article are included in the article's Creative Commons licence, unless indicated otherwise in a credit line to the material. If material is not included in the article's Creative Commons licence and your intended use is not permitted by statutory regulation or exceeds the permitted use, you will need to obtain permission directly from the copyright holder. To view a copy of this licence, visit <http://creativecommons.org/licenses/by-nc-nd/4.0/>.

© The Author(s) 2024